A Vertically Resolved Canopy Improves Chemical Transport Model Predictions of Ozone Deposition to North Temperate Forests

Michael P. Vermeuel[1,2,3] , **Dylan B. Millet[1]** , **Delphine K. Farmer[2]** , **Laurens N. Ganzeveld[4]**, **Auke J. Visser[4,5]** , **Hariprasad D. Alwe[6]**, **Timothy H. Bertram[7]** , **Patricia A. Cleary[8]** , **Ankur R. Desai[9]** , **Detlev Helmig[10]** , **Sarah C. Kavassalis[11]** , **Michael F. Link[2,12]** , **Matson A. Pothier[2,13]** , **Mj Riches[2]** , **Wei Wang[14]**, and **Sara Williams[2]**

[1]Department of Soil, Water, and Climate, University of Minnesota, St. Paul, MN, USA, [2]Department of Chemistry, Colorado State University, Ft. Collins, CO, USA, [3]Now at Department of Earth, Atmospheric, and Planetary Sciences, Purdue University, West Lafayette, IN, USA, [4]Meteorology and Air Quality Section, Wageningen University, Wageningen, The Netherlands, [5]Now at European Centre for Medium-Range Weather Forecasts (ECMWF), Bonn, Germany, [6]Tofwerk AG, Thun, Switzerland, [7]Department of Chemistry, University of Wisconsin–Madison, Madison, WI, USA, [8]Department of Chemistry and Biochemistry, University of Wisconsin–Eau Claire, Eau Claire, WI, USA, [9]Department of Atmospheric and Oceanic Sciences, University of Wisconsin–Madison, Madison, WI, USA, [10]Boulder A.I.R. LLC, Boulder, CO, USA, [11]Department of Chemistry, Harvey Mudd College, Claremont, CA, USA, [12]Now at Engineering Laboratory, National Institute of Standards and Technology, Gaithersburg, MD, USA, [13]Now at Aerodyne Research Inc., Billerica, MA, USA, [14]Institute of Arctic and Alpine Research, University of Colorado, Boulder, CO, USA

Abstract Dry deposition is the second largest tropospheric ozone (O_3) sink and occurs through stomatal and nonstomatal pathways. Current O_3 uptake predictions are limited by the simplistic big-leaf schemes commonly used in chemical transport models (CTMs) to parameterize deposition. Such schemes fail to reproduce observed O_3 fluxes over terrestrial ecosystems, highlighting the need for more realistic treatment of surface-atmosphere exchange in CTMs. We address this need by linking a resolved canopy model (1D Multi-Layer Canopy CHemistry and Exchange Model, MLC-CHEM) to the GEOS-Chem CTM and use this new framework to simulate O_3 fluxes over three north temperate forests. We compare results with in situ measurements from four field studies and with standalone, observationally constrained MLC-CHEM runs to test current knowledge of O_3 deposition and its drivers. We show that GEOS-Chem overpredicts observed O_3 fluxes across all four studies by up to 2×, whereas the resolved-canopy models capture observed diel profiles of O_3 deposition and in-canopy concentrations to within 10%. Relative humidity and solar irradiance are strong O_3 flux drivers over these forests, and uncertainties in those fields provide the largest remaining source of model deposition biases. Flux partitioning analysis shows that: (a) nonstomatal loss accounts for 60% of O_3 deposition on average; (b) in-canopy chemistry makes only a small contribution to total O_3 fluxes; and (c) the CTM big-leaf treatment overestimates O_3-driven stomatal loss and plant phytotoxicity in these temperate forests by up to 7×. Results motivate the application of fully online vertically explicit canopy schemes in CTMs for improved O_3 predictions.

Plain Language Summary Ozone is toxic to humans and plants and is also a potent greenhouse gas. A significant fraction of atmospheric ozone is removed via uptake to Earth's surface through the dry deposition process. Forests account for a large portion of global dry deposition through uptake into leaf pores and losses to leaf surfaces and soils. Atmospheric models generally calculate dry deposition using simple parameterizations that approximate forests as one big zero-dimensional leaf surface. However, this yields poor predictions of ozone deposition and surface concentrations. Here, we addressed this situation by linking a commonly used global atmospheric model to a one-dimensional canopy model that explicitly simulates chemistry and air transport through the forest airspace. We used this model hierarchy to simulate ozone concentrations and deposition over three forests and evaluated the results against observations. Results show that standard atmospheric models over predict ozone dry deposition by up to 2× and subsequent plant damage by up to 7×, but incorporation of an explicit canopy leads to excellent agreement with observations. Further, we found that ozone dry deposition within these canopies occurs primarily through leaf surfaces and soil uptake, and that chemical reactions within the canopy have only a minor impact on total ozone deposition.

1. Background

Tropospheric ozone (O_3) is a key atmospheric oxidant and the dominant source of hydroxyl radicals (OH). It is also a potent greenhouse gas (Stevenson et al., 1998, 2006) that is toxic to humans and plants. Elevated near-surface O_3 concentrations impair global health and food security, causing an estimated 365,000 premature deaths per year (Delang et al., 2021) and billions of dollars in annual agricultural losses (Avnery et al., 2011; Tai et al., 2014). Dry deposition to surfaces including leaves, soil, and water makes up an estimated 20% of the global tropospheric O_3 sink (Wild, 2007). The terrestrial biosphere accounts for over 85% of this deposition (Hardacre et al., 2015; Luhar et al., 2018) due to efficient irreversible uptake through plant stomata plus nonstomatal loss to other surfaces. Stomatal O_3 uptake causes oxidative damage that impairs a plant's ability to control transpiration and photosynthesis (Lombardozzi et al., 2012), thus reducing carbon assimilation and plant productivity (Ainsworth et al., 2012; Sitch et al., 2007) and altering the water cycle by decreasing latent heat fluxes and increasing runoff (Lombardozzi et al., 2015).

Atmospheric ozone predictions use chemical transport models (CTMs) that then inform decision-making aimed at controlling surface pollution and its negative health and ecological impacts. Dry deposition in CTMs is estimated using resistance-in-series "big-leaf" schemes that are based on empirical and computationally efficient parameterizations of canopy stomatal and nonstomatal losses (Wesely, 1989; Zhang et al., 2003). Differing implementations can lead to large O_3 deposition disparities among models (e.g., by up to threefold; Wong et al., 2019; Hardacre et al., 2015; Wu et al., 2018; Clifton et al., 2023), and significant biases have been identified in CTM-predicted surface ozone concentrations (e.g., up to 8 ppb; Young et al., 2018) and deposition fluxes (e.g., up to 30% overestimate in the Northern Hemisphere; Hardacre et al., 2015). Key model uncertainties arise in classifying land cover (Hardacre et al., 2015; Silva & Heald, 2018) and in parameterizing the dry deposition process itself (Visser et al., 2021; Wong et al., 2019; Wu et al., 2018)—in particular, its sensitivity to hydroclimate and photosynthesis (Kavassalis & Murphy, 2017; Lei et al., 2020; Lin et al., 2019; Sun et al., 2022; Wong et al., 2019, 2022).

Additional processes affecting surface ozone have been identified that are not generally included in CTMs or deposition models. For example, nonstomatal O_3 uptake can be enhanced when leaves are wet (Altimir et al., 2006; Rannik et al., 2012; Zhou et al., 2017) potentially due to reactions with dissolved organic carbon (Altimir et al., 2006; Ossola & Farmer, 2024; Sun et al., 2016). In-canopy gas-phase reactions with very reactive emitted volatile organic compounds (VOCs) and nitric oxide (NO) can occur on turbulent timescales and have also been found to account for a significant portion of surface O_3 removal (Fares et al., 2010; Goldstein et al., 2004; Kurpius & Goldstein, 2003; Rummel et al., 2007; Vermeuel et al., 2021). Meanwhile, turbulence is only roughly parameterized in deposition schemes but determines the efficiency of nonstomatal losses (El-Madany et al., 2017; Neirynck et al., 2012), whereas in-canopy vertical transport (not represented at all in CTMs) has been shown to control the offsetting effects of transport versus deposition on surface ozone (Visser et al., 2022).

One-dimensional canopy chemistry models provide a vertically resolved framework to explicitly represent the dry deposition, biogenic emissions, chemistry, and transport occurring within and above a forest canopy (Ashworth et al., 2015; Bryan et al., 2012; Ganzeveld et al., 2002b; Wolfe & Thornton, 2011). Since within-canopy air experiences different environmental conditions than does the overlying atmosphere, this enables a more physically accurate treatment of near-surface loss processes than is possible with zero-dimensional CTM deposition schemes. The effects can be significant: Makar et al. (2017) found that the absence of foliage-modified shading and in-canopy vertical diffusion in 3D CTMs biased North American surface O_3 forecasts by up to 72%.

To date, one-dimensional canopy chemistry models have mostly been used in a standalone configuration to investigate the mechanisms controlling fluxes and surface concentrations of O_3, NO_x, and VOCs (Clifton et al., 2023; Seok et al., 2013; Visser et al., 2021, 2022; Wolfe et al., 2011; Yanez-Serrano et al., 2018; Zhou et al., 2017). The Multi-Layer Canopy-CHemistry Exchange Model (MLC-CHEM) is one such model that is well suited for CTM implementation due to its efficient configuration and state-of-science treatment for relevant dry deposition processes (Ganzeveld et al., 2002b, 2002c; Visser et al., 2021, 2022). In particular, MLC-CHEM predicts stomatal uptake using a physiologically realistic semiempirical photosynthesis-stomatal parameterization (Ronda et al., 2001) and explicitly resolves nonstomatal deposition to bare, wet, snow, and vegetative surface fractions. MLC-CHEM has previously been implemented online in the chemistry-climate ECHAM/MESSy

Atmospheric Chemistry (EMAC) model to study the impact of land cover and land use changes on chemistry and climate (Ganzeveld et al., 2010).

Here, we investigate the extent to which a resolved-canopy representation can improve CTM predictions of surface O_3 concentrations and forest-atmosphere exchange. To this end, we use a hierarchy of models to interpret a comprehensive suite of chemical observations from four field studies over three north temperate forests. The model set includes the GEOS-Chem 3D CTM, an observationally constrained standalone implementation of the MLC-CHEM 1D canopy model, and a one-way coupled framework that drives the MLC-CHEM resolved canopy with parameters from a parent GEOS-Chem CTM. We interpret the model measurement comparisons in terms of the ability of the different simulations to represent the observed O_3 fluxes and concentrations and to better understand the fate and ecological impacts of surface O_3. Results from this analysis are used to assess the utility of incorporating a fully coupled resolved canopy into the GEOS-Chem CTM.

2. Methods

2.1. Site Descriptions and Observations

We use data from three north temperate forests acquired during four seasonal field studies to test our understanding of O_3 surface-atmosphere exchange and its representation in atmospheric models. The following sections briefly describe the measurement sites and associated chemical and meteorological observations used in the ensuing analyses. Tables S1 and S2 in Supporting Information S1 outline all acronyms and variables used in this remainder of this text.

2.1.1. The Flux Closure Study (FluCS) 2021

FluCS 2021 (Vermeuel, Millet, et al., 2023) took place from 6 August to 25 September 2021 at the Manitou Experimental Forest Observatory (MEFO) in the Colorado Front Range (39.101°N, 105.094°W, 2370 m elevation) over a semiarid montane forest composed primarily of ponderosa pine (∼15 m height), shrubs, and grassland. The summertime leaf area index (LAI) within the flux footprint was 2.4 m^2 m^{-2} (Vermeuel, Millet, et al., 2023). Meteorological observations during FluCS 2021 included 3D winds and temperatures recorded from three heights (6.9, 14.6, and 27.8 m) on the 28 m MEFO tower and photosynthetically active radiation (PAR) measured near-ground. Concentrations of O_3, NO_x, CO_2, and H_2O were quantified at five heights (3.2, 6.9, 10.6, 14.6, and 19.8 m). In addition, net ecosystem VOC, CO_2, sensible heat, latent heat, and O_3 fluxes were measured at 27.8 m by eddy covariance (EC) (Stull, 1988). The VOC fluxes were quantified using two high-resolution time-of-flight mass spectrometers (HR-ToFMS): a proton-transfer reaction mass spectrometer (PTRMS; PTR-QiToF, Ionicon Analytik) and an iodide anion (I^-) chemical ionization mass spectrometer (ICIMS; HR-ToF-MS, Aerodyne Inc.). Speciated VOC measurements were also collected in ambient air and at the leaf level to characterize ponderosa pine and understory vegetative emissions (Riches et al., 2024). Ozone fluxes were measured by ICIMS as described next. We direct the reader to Vermeuel, Millet, et al. (2023) for more details on other FluCS 2021 measurements.

The ICIMS was used to quantify O_3 concentrations and EC fluxes at 27.8 m using the total IO_x^- signal ($x = 1$–3), which accounts for the major secondary reactions of O_3 product ions within the ICIMS (Supporting Information S1.1) (Bhujel et al., 2020; Dörich et al., 2021; Teiwes et al., 2019). We calibrated the ICIMS IO_x^- signal during FluCS against simultaneous measurements from a UV photometric O_3 analyzer along the five lower inlet heights; the two data sets were tightly correlated throughout the campaign (Figure S1 in Supporting Information S1). Furthermore, the above-canopy to mid-canopy O_3 concentration gradients derived from the two instruments agreed to within 5% during daytime when deposition was strongest (Figure S2 in Supporting Information S1), supporting the robustness of the ICIMS-measured fluxes. Dörich et al. (2021) report that high HNO_3 signals (as NO_3^-) can affect the O_3 calibration at IO_x^-, but we did not see such an effect—presumably due to low ambient HNO_3 and its loss in the 45 m inlet (Figure S1 in Supporting Information S1). There were also no quantifiable O_3 interferences from I^- and IO^- reactions with organic acids (Supporting Information S1.1; Figure S3 in Supporting Information S1), which have been previously reported at high acid concentrations (Zhang & Zhang, 2021) and would be expected to cause correlations between peracetic acid and O_3. The ICIMS ion-molecule reactor was humidified ($[H_2O]_{IMR} \approx$ 10 parts per thousand; $\overline{[H_2O]_{ambient}}$ = 9.1 parts per thousand) (Link et al., 2024), mitigating any sensitivity changes due to ambient water fluctuations (Supporting

Information S1.1). The resulting EC O_3 fluxes were filtered using appropriate quality control criteria (Foken & Wichura, 1996; Lee et al., 2005; Mauder et al., 2013) (Supporting Information S1.2); high-frequency flux attenuation was minor (3.1%; Figure S4 in Supporting Information S1) (Horst, 1997) and therefore no correction was applied. We estimated the average flux uncertainty at 18% using the flux limit of detection method described by Langford et al. (2015). More details on the ICIMS measurements during FluCS 2021 are provided by Link et al. (2024).

2.1.2. Program for Research on Oxidants: Photochemistry, Emissions, Transport—Atmospheric Measurements of Oxidants in Summer (PROPHET-AMOS)

The PROPHET-AMOS study took place throughout 2016 July at the University of Michigan Biological Station near the north end of the lower peninsula of MI, USA (45.559°N, 84.715°W, 232 m elevation). The surrounding mixed forest is primarily deciduous (Seok et al., 2013) with an average satellite-derived LAI of 3.7 $m^2\,m^{-2}$ for the PROPHET-AMOS measurement period. The chemical and micrometeorological data sets during this study were collected at two towers: the 34 m PROPHET tower located at the coordinates above, and the 46 m US-UMB Ameriflux tower (45.560°N, 84.714°W, 234 m elevation; Gough et al., 2013), ~130 m northeast of the PROPHET tower. Data from the PROPHET tower used in the present study include above-canopy (34 m) VOC fluxes (PTR-QiToF; Millet et al., 2018; Alwe et al., 2019) and 3D winds and temperatures measured using sonic anemometers installed at six heights within and above the forest canopy (34, 29, 21, 13, and 5 m) (Bui et al., 2021). We also use O_3 and NO_x concentration gradients measured from 10 positions along the US-UMB tower between 0.6 and 27.4 m (Univeristy of Michigan, 2023). Finally, we use a suite of Ameriflux meteorological data (relative humidity, RH; temperature; solar radiation; windspeed; latent and sensible heat; and friction velocities) measured at 46 m on the US-UMB tower (Gough et al., 2023). We assume surface homogeneity between the towers based on their proximity and the temporally coherent above-canopy friction velocities ($r^2 = 0.87$) and sensible heat fluxes ($r^2 = 0.85$) observed at the two sites.

2.1.3. The Chequamegon Heterogeneous Ecosystem Energy-Balance Study Enabled by a High-Density Extensive Array of Detectors 2019 (CHEESEHEAD19)

The CHEESEHEAD19 (C19) field study was conducted in the Chequamegon-Nicolet National Forest near Park Falls, WI, amid a landscape that primarily consists of woody wetlands along with some grasslands and deciduous + evergreen forests (Butterworth et al., 2021). The site has a mean canopy height of 15 m with a 2019 July satellite-derived LAI of 5.3 $m^2\,m^{-2}$. For our analysis, we use Ameriflux meteorological data collected from 30 m at the US-PFa site in Park Falls, WI (45.945°N, 90.273°W, 472 m elevation; Davis et al., 2003) during CHEESEHEAD19 (Desai, 1996). Additional observations during this study included O_3 concentrations measured continuously at two heights (30 and 122 m) from 3–15 July 2019 using both a UV photometric analyzer (Vermeuel et al., 2021) and an oxygen anion (O_2^-) CIMS (Ox-CIMS) (Novak et al., 2020). The Ox-CIMS was also used to quantify O_3 fluxes by EC at 30 m for 6 days during CHEESEHEAD19 with details provided by Vermeuel et al. (2021).

2.1.4. Probing Ecosystem Responses Involving Notable Organics (PEcoRINO)

The fourth data set used in this analysis is from the PEcoRINO study that took place at the US-PFa site in 2020 September. Chemical observations were collected at 30 m, including VOC concentrations and EC flux measurements using a PTRMS (Vocus; Aerodyne Research Inc. and Tofwerk AG) and O_3 concentrations using a UV photometric analyzer (Vermeuel, Novak, et al., 2023). The PTRMS was coupled to a gas chromatograph for periodic online VOC speciation (Claflin et al., 2021). We use Ameriflux meteorological data collected at 30 m during the study period (Desai, 1996). Data used here are restricted to 06-16 September—during the growing season (as determined from phenological observations and satellite-based LAI >2 $m^2\,m^{-2}$) and prior to the senescence-related VOC enhancements documented by Vermeuel, Novak, et al. (2023).

2.2. Model Descriptions

2.2.1. GEOS-Chem

We use the GEOS-Chem CTM v13.3.0 (The International GEOS-Chem User Community, 2021) to interpret the above observations in terms of the information they provide on O_3 deposition processes and their representation in
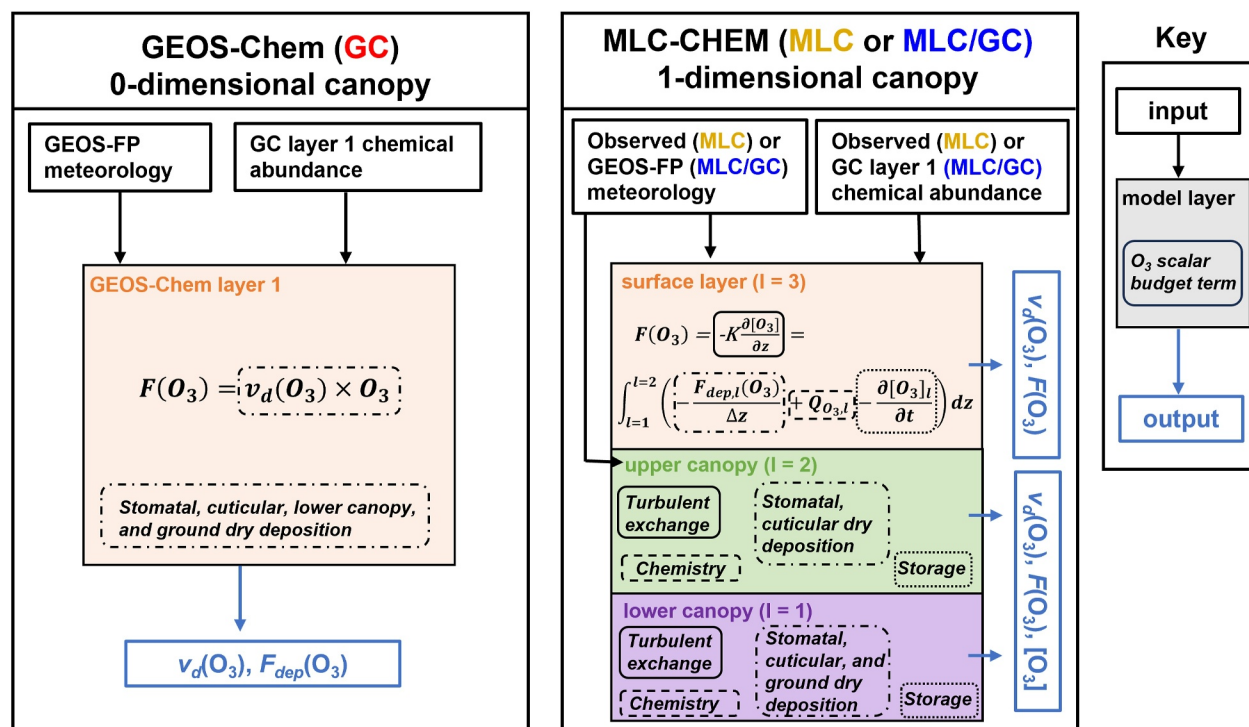
Figure 1. Generalized deposition schemes for (a) GEOS-Chem (GC) and (b) MLC-CHEM (MLC and MLC/GC) simulations. GEOS-Chem derives the ozone flux (F(O_3)) using a dimensionless dry deposition parameterization constrained by meteorological and chemical information from the first model layer. Our implementation of MLC-CHEM resolves a forest into two underlying canopy layers ($l = 1,2$) and solves for F(O_3) as the vertical turbulent flux via Equation 2. MLC runs are constrained to observations, whereas MLC/GC runs are constrained using GEOS-FP meteorological and GEOS-Chem chemical fields. Box outline styles identify individual scalar budget contributions to F(O_3).

3D models. The GEOS-Chem implementation used here employs assimilated meteorology (Goddard Earth Observation System Forward Processing product; GEOS-FP) from the NASA Global Modeling and Assimilation Office, which has $0.25° \times 0.3125°$ native horizontal resolution, 72 vertical layers, 3-hr temporal resolution for 3-D meteorological parameters, and 1-hr temporal resolution for surface quantities and mixing depths. We performed $0.25° \times 0.3125°$ full-chemistry simulations over custom nested domains surrounding each observation site ($\pm 3°$ latitude and longitude) and for the duration of the corresponding field study. These nested simulations employed 5 and 10 min time steps for transport and chemistry, respectively (Philip et al., 2016). Boundary conditions were taken from $2° \times 2.5°$ global model runs for the same time periods that were themselves initialized using output from a yearlong global simulation at $4° \times 5°$. Simulations for FluCS are the same as those described by Vermeuel, Millet, et al. (2023).

The full chemistry GEOS-Chem chemical mechanism used here features comprehensive HO_x-NO_x-O_x-VOC-Br-Cl-I chemistry coupled to aerosols and incorporates recent JPL/IUPAC recommendations. It includes chemical updates for isoprene oxidation (Bates & Jacob, 2019), small oxygenated VOCs (Bates et al., 2021; Chen et al., 2019), halogens (Wang et al., 2019), small alkyl nitrates (Fisher et al., 2018), sesquiterpenes (SQT), 2-methyl-3-buten-2-ol (232-MBO), and >C2 organic acids (Vermeuel, Millet, et al., 2023). Surface emissions are incorporated using the Harmonized Emissions Component module version v3 (Lin et al., 2021) with emissions from terrestrial plants computed online using the Model of Emissions of Gases from Nature (MEGAN) (Guenther et al., 2012) as implemented by Hu et al. (2015) and soil NO_x emissions following Hudman et al. (2012). Anthropogenic emissions are obtained from the Community Emissions Data Systems inventory (Hoesly et al., 2018) and biomass burning emissions from the Global Fire Emissions Database v4 (Giglio et al., 2013). Lightning NO_x, aircraft, and ship emissions are computed using the standard GEOS-Chem inventories (Holmes et al., 2014; Murray et al., 2012; Stettler et al., 2011).

GEOS-Chem estimates dry deposition for a given gas as the product of its concentration in the first model layer times its calculated deposition velocity (v_d; cm s^{-1}) (Figure 1a). The model uses the Wesley (1989) (hereafter

W89) dimensionless big-leaf deposition scheme that conceptualizes the forest canopy as a single surface and calculates v_d based on in-series aerodynamic, boundary layer, and canopy resistances (r_a, r_b, r_c, respectively; s cm^{-1}):

$$v_d = (r_a + r_b + r_c)^{-1}. \tag{1}$$

The r_c value encompasses four individual resistances (for stomatal, cuticular, lower canopy, and ground surface deposition) summed in parallel, each parameterized using land-type lookup values and associated physical dependencies. The GEOS-Chem r_c algorithm has been adapted from W89 for global use and incorporates modifications for canopy radiative transfer (Baldocchi et al., 1987; Wang et al., 1998). Computation of r_c is based on the summation in parallel of: (a) stomatal (r_s) + mesophyll (r_m) resistance; (b) plant cuticle resistance (r_{cut}); (c) lower canopy (r_{cl}) + in-canopy convection (r_{dc}) resistance; and (c) ground (r_g) + ecosystem-specific in-canopy turbulence (r_{ac}) resistance:

$$r_c = \left(\frac{1}{r_s + r_m} + \frac{1}{r_{cut}} + \frac{1}{r_{dc} + r_{cl}} + \frac{1}{r_{ac} + r_g} \right)^{-1}. \tag{2}$$

A more detailed breakdown of the resistances controlling $v_d(O_3)$ in W89 and GEOS-Chem is provided in Supporting Information S1 and by Clifton et al. (2023).

2.2.2. MLC-CHEM

We use the 1D MLC-CHEM canopy-chemistry model to perform vertically resolved simulations of forest-atmosphere exchange at our four field sites. MLC-CHEM simulates vertical concentration and flux profiles explicitly by solving trace gas tendencies at each layer within a model canopy. In the case of O_3 we thus have:

$$\frac{d[O_3]_l}{dt} = -\frac{\Delta F_{turb,l}}{\Delta z_l} - \frac{F_{dep,l}}{\Delta z_l} + Q_{O_3,l}, \tag{3}$$

where Δz_l is the model layer thickness, $-\frac{\Delta F_{turb,l}}{\Delta z_l}$ is the vertical turbulent flux divergence, $F_{dep,l}$ is the dry depositional flux, and $Q_{O_3,l}$ is the net chemical production or loss of O_3 all computed for each model layer l. The vertical turbulent flux is derived from first-order closure theory:

$$F_{turb,l} = -K_{H,l} \frac{\Delta[O_3]_l}{\Delta z_l}, \tag{4}$$

where $K_{H,l}$ is the heat eddy diffusivity (m^2 s^{-1}). The dry depositional flux in each layer is calculated using a resistance-in-series parameterization (Equation 1) (Ganzeveld et al., 1998; Ganzeveld & Lelieveld, 1995; Visser et al., 2021).

Resistance to leaf uptake in layer l is computed as

$$r_{leaf,l} = \frac{r_{b,leaf} + \left(\frac{1}{r_{s,l}} + \frac{1}{r_{cut,l}} \right)^{-1}}{\max \left\{ LAI_l, 10^{-5} \right\}}, \tag{5}$$

where $r_{b,leaf}$ is the resistance to transport across the quasi-laminar leaf boundary layer. In the upper canopy layer ($l = 2$), r_c reflects leaf uptake only whereas in the lower canopy layer ($l = 1$) ground uptake and leaf uptake occur in parallel:

$$r_{c,1} = \left(\frac{1}{r_{leaf,1}} + \frac{1}{r_{ac} + r_g} \right)^{-1}. \tag{6}$$

Here, we calculate stomatal loss with an assimilation-stomatal conductance (A-g_s) model (Ronda et al., 2001) using ecosystem-specific parameters from Visser et al. (2021) (Supporting Information S2.2). We validate this parameter choice based on a comparison of simulated and observed above-canopy CO_2 fluxes, which agree to within 25% on average. Nonstomatal removal is estimated using W89 landtype-dependent resistances for soil and cuticular loss. We update the modeled cuticular uptake to wet leaves by inferring the wet fraction (f_{wet}) from RH (Lammel, 1999) as implemented in MLC-CHEM (Visser et al., 2021). Further details on the MLC-CHEM dry deposition calculations are presented in Supporting Information S2.2. Chemical tendencies are solved in each layer using the carbon bond mechanism IV (CBM IV) scheme, whereas biogenic emissions are calculated using the MEGAN and Yienger and Levy (1995) parameterizations for plant VOCs and soil NO, respectively.

We configure MLC-CHEM as shown in Figure 1 with an atmospheric surface layer, an upper canopy layer, and a lower canopy layer; the latter two each comprise one-half of the total canopy height. We first simulate radiation-dependent process, including biogenic emissions for four canopy sublayers that are then averaged over the two MLC-CHEM canopy layers. This approach has been shown to represent atmosphere-biosphere exchange of O_3 and other trace gases as accurately as models with much higher vertical resolution (Ganzeveld et al., 2002a). Here, we perform two MLC-CHEM runs for each field study: one (hereafter referred to as MLC) constrained by meteorological and chemical observations at that site and one (referred to as MLC/GC) constrained by meteorological data and trace gas mixing ratios from GEOS-FP/GEOS-Chem. The corresponding CTM-only GEOS-Chem runs are referred to as GC in what follows.

MLC-CHEM is forced using hourly observed (for MLC runs) or GEOS-FP (for MLC/GC runs) surface-layer RH, solar radiation, temperature, wind speed, and friction velocity (u_*). Surface-layer O_3 and NO_x concentrations are nudged to their observed (MLC) or parent-model (MLC/GC) values. Table S3 in Supporting Information S1 outlines the observations available for each MLC simulation. The MLC-CHEM surface layer uses a simplified bulk planetary boundary layer (PBL) representation with transport computed between the middle of the PBL and the middle of the upper canopy layer. For the observationally constrained MLC runs, we therefore first obtain the surface-layer K_H ($K_{H,sl}$) values from the observed sensible heat fluxes and scale $K_{H,sl}$ to the mid-PBL (altitude derived from GEOS-FP) by assuming a linear height dependence within this range. We then derive canopy-layer K_H ($K_{H,cl}$) values from measurements at the upper/lower canopy interface; when such data is not available we instead compute $K_{H,cl}$ by scaling the observational $K_{H,sl}$ values to a prescribed in-canopy profile that increases exponentially with height (Cionco, 1972; Harman & Finnigan, 2007; Visser et al., 2022).

For the model-constrained MLC/GC runs, we obtain $K_{H,sl}$ by linearly scaling the GEOS-FP layer-1 K_H values to the mid-PBL; $K_{H,cl}$ is then computed from $K_{H,sl}$ as above. The GEOS-FP RH values were scaled by 1.2× to better match surface observations; we attribute the discrepancy to the fact that the GEOS-FP values reflect the average over a ≥100 m vertical layer (and across a heterogenous 0.25° × 0.3125° grid cell) as opposed to the local near-canopy environment. The observed (MLC) and GEOS-FP (MLC/GC) meteorological fields then generally agree well, including (of particular relevance for simulating deposition) the surface-layer and in-canopy K_H values (Figure 2, Figure S5 in Supporting Information S1). There is a 1.5× GEOS-FP photosynthetic photon flux density (PPFD) overestimate in the case of the FluCS runs, which we attribute to inhomogeneity in sunlit fraction for terrain in the surrounding model grid cell.

Concentrations of O_3, NO_x, and VOCs are provided as chemical constraints to the MLC and MLC/GC model runs. In the case of MLC/GC, the surface-layer O_3 concentrations are nudged to the corresponding GEOS-Chem values, which means we are technically overcounting the impact of local deposition (i.e., at our site) on the overlying O_3 field. However, a comparison of GC surface-layer O_3 concentrations across the model grid cells surrounding our field site reveals a coefficient of deviation of <5%. This implies that above-canopy O_3 concentrations are regionally controlled and more affected by upwind processes than by immediate local effects in keeping with the ∼3 days GC lifetime for O_3 surface uptake in these grid cells. Constraining the MLC/GC surface-layer O_3 concentrations based on the corresponding GC values is thus a suitable approximation; a future fully online MLC implementation within GC would fully avoid any such overcounting.

Although all field studies included above-canopy O_3 observations, only the FluCS and PROPHET campaigns featured above-canopy NO_x measurements. MLC analyses for the remaining studies are instead constrained to the GC surface-layer NO_x values. A model-measurement comparison for NO_x at PROPHET reveals a 2.5× GC high bias; given the regional and ecological similarity of the PROPHET and CHEESEHEAD19/PEcoRINO sites this implies that the corresponding model runs provide an upper limit for in-canopy O_3 loss to NO. Emissions of
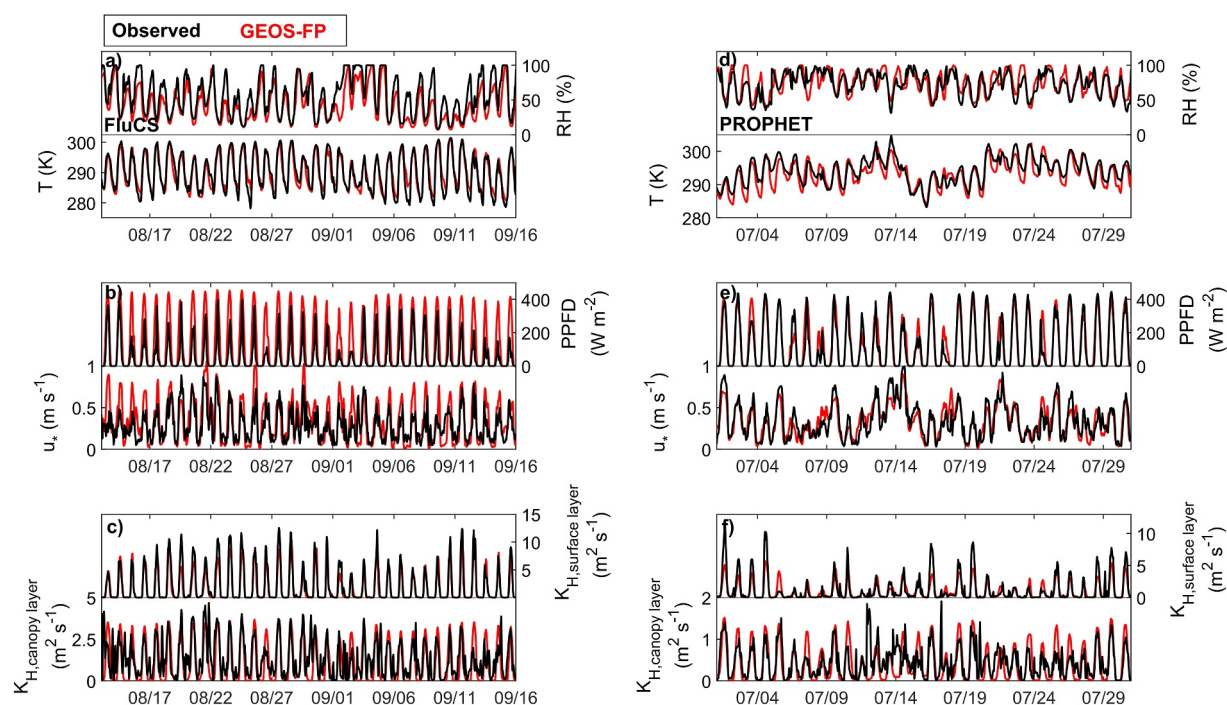
Figure 2. Observed (black lines) and assimilated (GEOS-FP, red lines) meteorological fields during the (a–c) FluCS and (d–f) PROPHET studies. The corresponding data for CHEESEHEAD19 and PEcoRINO are shown in Figure S5 in Supporting Information S1.

isoprene (C_5H_8), monoterpenes (MT; $C_{10}H_{16}$), and sesquiterpenes (SQT; $C_{15}H_{24}$) are prescribed using canopy-level emission factors from MEGAN v2.1 (for GC runs) or using leaf-level emission factors observed on-site (for MLC and MLC/GC). For the FluCS MLC and MLC/GC runs, we also account for 232-MBO, which made up 66% of the total observed OH reactivity-weighted VOC flux (i.e., the OH reactivity flux) during the study (Vermeuel, Millet, et al., 2023). Specifically, for the MLC and MLC/GC FluCS runs, we scaled the model isoprene emission factors to also include 232-MBO with the latter flux weighted by the $k_{OH+232\text{-}MBO}{:}k_{OH + isoprene}$ ratio (~0.4 at 298 K) (Fantechi et al., 1998; Karl et al., 2004). To maintain consistency with the above-canopy constraints in each case, we then scaled the leaf-level emission factors uniformly so that the simulated surface-layer fluxes matched the above-canopy observations (for MLC) or GC-derived emissions (for MLC/GC). CHEESEHEAD19 lacked VOC flux observations, and in that case we apply emission factors from PEcoRINO since the two campaigns occurred at the same site.

All model simulations treat MT as a single isomer, which by default we implement based on α-pinene since it had the median O_3 reactivity ($\tau_{30\,ppb\,O_3}$ = 4.6 hr; Atkinson & Arey, 2003) across all MT isomers detected during FluCS (Riches et al., 2024; Vermeuel, Millet, et al., 2023) and PEcoRINO (Vermeuel, Novak, et al., 2023). Sensitivity simulations were also performed instead treating all MT as β-ocimene (the most reactive isomer identified in the field studies; $\tau_{30\,ppb\,O_3}$ = 44 min); we will show in Section 3.5 that this had negligible effect on the computed in-canopy O_3 loss. SQT chemistry is modeled based on β-caryophyllene, providing an upper limit for the resulting O_3 reactivity given its short lifetime ($\tau_{30\,ppb\,O_3}$ = 2 min).

3. Results and Discussion

3.1. Near-Surface O_3 Fluxes and Concentrations Are Well-Represented in an Observationally Constrained Canopy Model

Figure 3 summarizes the observed and simulated O_3 fluxes and concentrations during our four field studies. The measured fluxes and $v_d(O_3)$ values from FluCS and CHEESEHEAD19 (C19) peak on average near 11:00 local time (LT) concurrent with the high RH and solar radiation that together maximize stomatal conductance (g_s). The constrained MLC simulations likewise predict a late-morning $v_d(O_3)$ peak across all four field studies with the
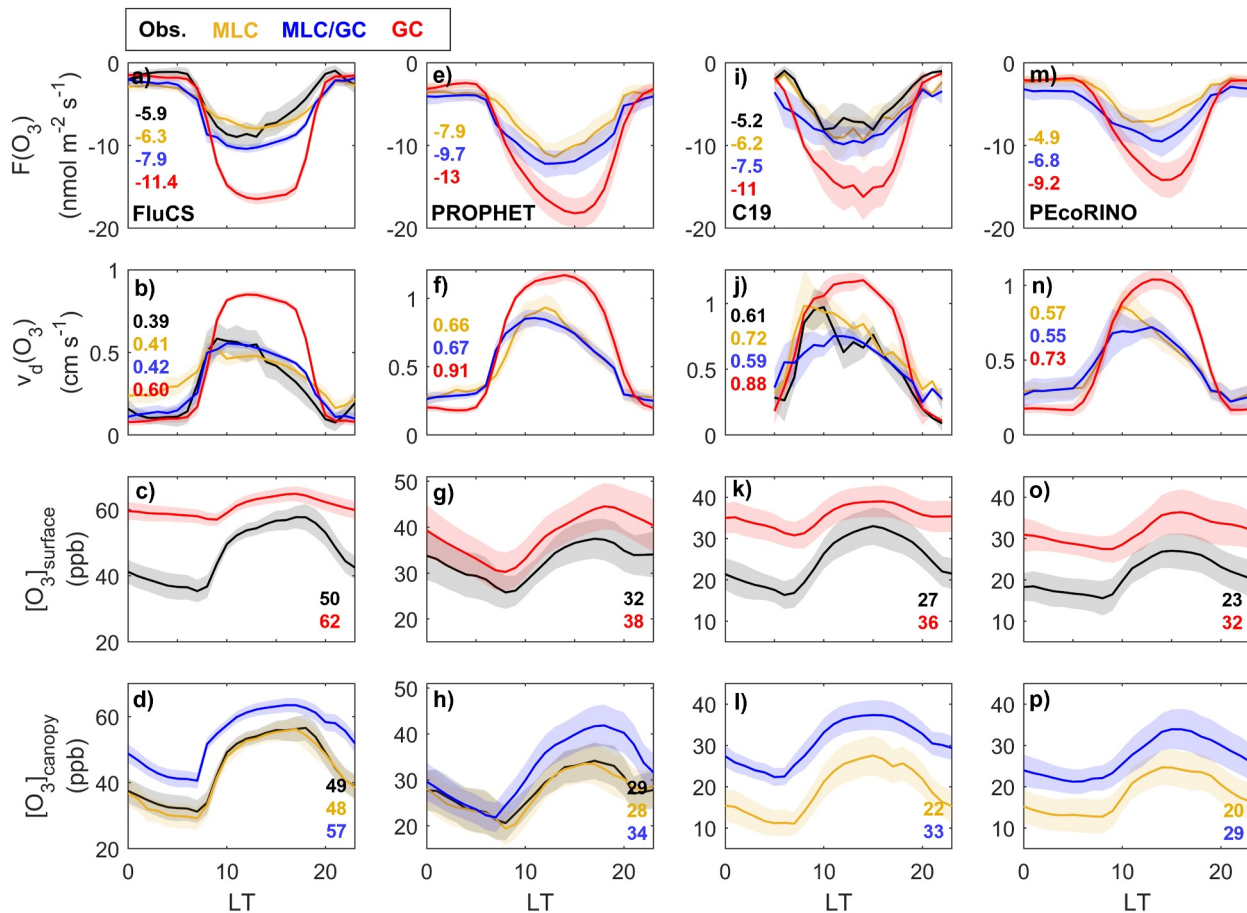
Figure 3. Diel O_3 fluxes ($F(O_3)$), deposition velocities ($vd(O_3)$), surface layer concentrations, and in-canopy concentrations for four field studies. Observed (Obs.) and model-predicted (MLC, MLC/GC, GC) data are plotted for the FluCS (a–d), PROPHET (e–h), C19 (i–l), and PEcoRINO (m–p) campaigns. Lines and shaded regions show the diel means with associated 95% confidence intervals. Daytime mean values (7–19 LT) are listed inset.

strong daytime model-measurement $v_d(O_3)$ agreement at sites featuring O_3 flux observations (to within 8% for FluCS and 20% for C19) showing that the A-g_s stomatal conductance framework in MLC accurately captures the integrated effects of stomatal uptake. The in-canopy diel O_3 cycles predicted by MLC also agree well (to within 1 ppb) with the observed values (available at FluCS and PROPHET-AMOS; Figure 3). MLC overpredicts the measured O_3 fluxes and $v_d(O_3)$ values for FluCS at night (Figure 3a) due to (a) nonnegligible nocturnal in-canopy K_H, which enhances lower-canopy and ground loss and (b) concurrently high RH, which enhances cuticular loss (Figures 2a and 2c). An MLC soil resistance underestimate is also a possibility but if present would have only a small effect on nocturnal O_3 loss at FluCS (e.g., evening $v_d(O_3)$ values decrease by just 5% with $r_{soil} = 400$ s m^{-1} versus the default 200 s m^{-1}). Overall, the overestimated O_3 uptake at night leads to a modest MLC underestimate of in-canopy O_3 during early morning at this site. This suggests that our treatment of nonstomatal conductance (g_{ns}) overestimates the physical and chemical loss of O_3 to wet needle leaves and to the nocturnal understory/soils at this particular site.

Day-to-day flux differences are also seen at these sites, reflecting the influence of environmental drivers and providing an avenue for testing model processes. At FluCS, Figure 4 shows that the observations exhibit a high degree of variability, with coefficients of variation (CV; standard deviation divided by mean) of ~0.6 for the daytime-average (7:00-19:00 LT) O_3 fluxes and $v_d(O_3)$ values. Some of the day-to-day variability in $v_d(O_3)$ and $[O_3]_{surface}$ is explained by vapor pressure deficit (VPD) and PPFD fluctuations ($r^2 = 0.19$–0.30), reflecting the role of g_s-controlled deposition. Otherwise, the daytime-mean O_3 fluxes and $v_d(O_3)$ values do not show a clear dependence on any single meteorological driver ($r^2 < 0.1$ in all cases).
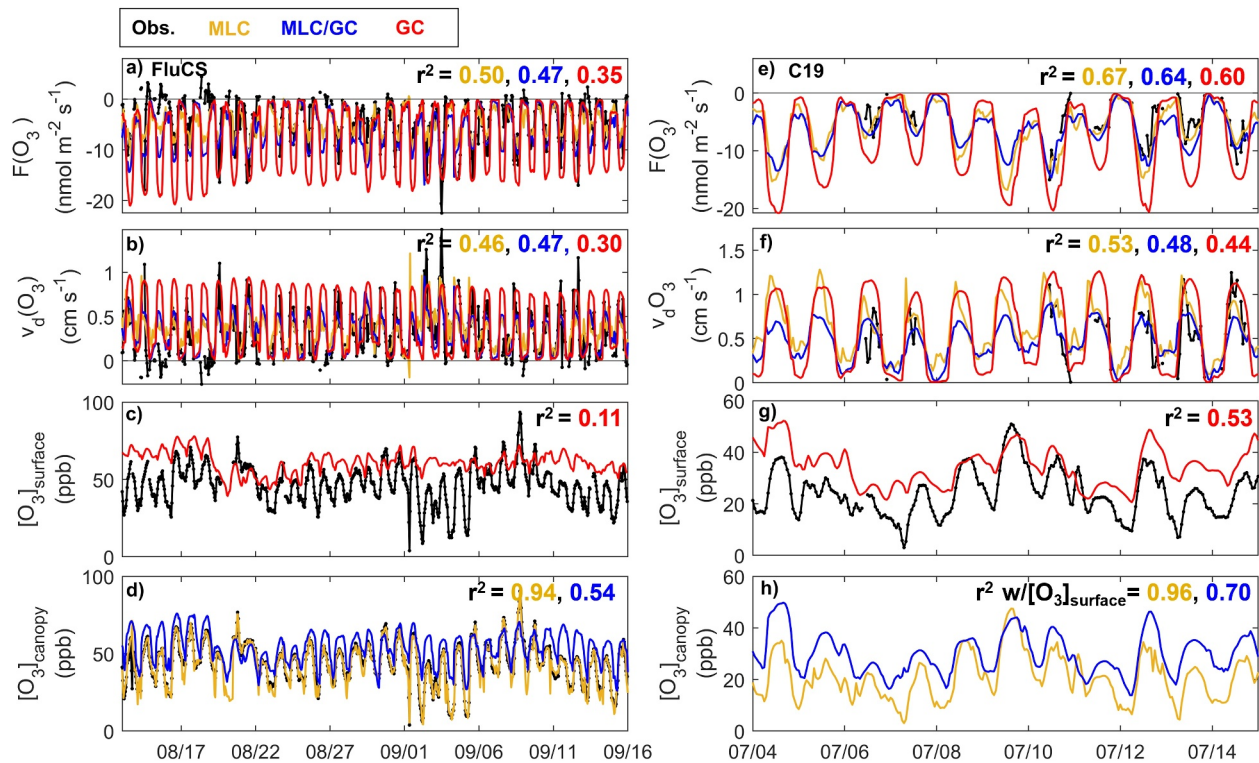
Figure 4. Hourly O_3 fluxes ($F(O_3)$), deposition velocities ($vd(O_3)$), surface layer concentrations ($[O_3]_{surface}$), and mean canopy concentrations ($[O_3]_{canopy}$) for the FluCS (a–d) and C19 (e–h) field studies. Observed (Obs.) and modeled (MLC, MLC/GC, GC) data are shown. Model versus observation coefficients of determination (r^2) are listed inset and colored by model run. For panel h, model $[O_3]_{canopy}$ values are regressed against observed $[O_3]_{surface}$ values. Scales of y-axes differ across sites.

The corresponding MLC simulations likewise show substantial daytime flux variability (CV ~ 0.4; Figures 4a and 4b). These daytime-mean $v_d(O_3)$ predictions are mostly driven by VPD and RH ($r^2 \sim 0.70$); the fact that such a clear dependence is not seen in the observations implies that the MLC treatment of stomatal (VPD-parameterized) and nonstomatal (RH-parameterized) uptake does not capture their full complexity at this site. The resulting MLC flux predictions reproduce about half of the day-to-day changes that are observed ($r^2 = 0.50$).

At C19, the observed O_3 fluxes and $v_d(O_3)$ values have moderate day-to-day variability (CV ~0.40) with a stronger direct dependence on VPD, PPFD, u_*, and horizontal windspeed (U) ($r^2 = 0.37–0.70$) than is seen at FluCS. The surface O_3 concentrations during C19 and PEcoRINO are positively correlated with u_* and U ($r^2 > 0.60$), showing that transported O_3 pollution enhances the downward fluxes in this region. The constrained MLC predictions at C19 are broadly similar to the observations in terms of their dependence on environmental drivers: the daytime-mean MLC $v_d(O_3)$ values correlate strongly with VPD and RH ($r^2 \sim 0.70$) while the fluxes depend on u_* ($r^2 = 0.50$) in-line with the measured relationships. This similarity between the MLC-predicted and observed relationships shows that the dry deposition and vertical transport parameterizations used in MLC-CHEM better represent the physical and chemical canopy processes at US-PFa (C19 and PEcoRINO) than at MEFO (FluCS), and as a result the day-to-day flux differences are also better captured at this site (Figure 4).

From the above results, we see that MLC represents the O_3 deposition observed at these sites with minimal bias (<20% in the 24-hr mean) while accurately predicting the diel flux, $v_d(O_3)$, and concentration profiles. The simulations also reproduce over half of the observed day-to-day variability in each case, indicating that MLC-CHEM captures many of the complex drivers controlling surface O_3. Patterns of variability that remain unexplained may reflect incomplete treatments of g_{ns} and g_s, or periods when vertical transport does not adhere to the first-order closure assumptions embedded in MLC-CHEM. Overall, however, the model-measurement comparisons across these sites demonstrate that MLC is a viable tool for predicting the fate of near-surface O_3 and for diagnosing the micrometeorological and biological drivers of its variability.

3.2. A Chemical Transport Model With Standard Big-Leaf Canopy Fails to Reproduce Observed O_3 Fluxes and Concentrations

In contrast to MLC, the big-leaf treatment in GEOS-Chem (GC) fails to capture both the magnitudes and diel cycle of the observed O_3 fluxes and $v_d(O_3)$ values. First, Figure 3 shows that GC overestimates the ozone fluxes by up to 2× compared to the observations and MLC at all sites. This bias arises from a $v_d(O_3)$ overestimate of up to 1.5× combined with a 15%–40% overestimate of the surface O_3 concentrations. Second, the $v_d(O_3)$ diel profile predicted by GC misses the g_s-driven morning peak that is observed at FluCS and C19, and captured by MLC at all sites. GC instead simulates a sustained $v_d(O_3)$ plateau from 11 to 16 LT that scales with site LAI, revealing an inadequate sensitivity of the W89 parameterization to daytime meteorological drivers that has likewise been identified in other studies (Clifton et al., 2023; Visser et al., 2021; Wu et al., 2018). The resulting GC-simulated fluxes then peak with $[O_3]_{surface}$ later in the day—a behavior inconsistent with the observations and with MLC. Furthermore, the $[O_3]_{surface}$ diel amplitude predicted by GC is too weak for all cases except PROPHET with the observed nighttime $[O_3]_{surface}$ decrease underestimated by >10 ppb (Figure 3). This shows that a CTM lacking near-surface vertical transport and in-canopy O_3 sinks incorrectly represents the O_3 vertical gradient and concentrations near ground level.

Figure 4 shows that GC also predicts less day-to-day flux and $v_d(O_3)$ variability than is observed (daytime-mean CVs of ~0.2 vs. 0.4–0.6 at FluCS and C19, where such observations are available), showing that GC does not represent the underlying processes as well as MLC. Low daytime $v_d(O_3)$ variability is also simulated by GC for PROPHET and PEcoRINO (CVs of 0.15 and 0.22, respectively). The GC-simulated fluxes and $v_d(O_3)$ values have a much stronger correlation with u_* ($r^2 = 0.40$–0.70) than is observed, showing that O_3 uptake in GC is primarily limited by transport and depositional area (i.e., LAI) and is less sensitive to other processes that also affect deposition. This lack of sensitivity to other meteorological drivers implies that GC will underpredict the impacts on O_3 deposition from future environmental changes—for example, rising ambient temperatures or VPD increases associated with drought.

3.3. A Resolved Canopy With Updated Dry Deposition Parameterizations Significantly Improves CTM O_3 Predictions

The MLC/GC runs that include a resolved canopy reproduce the observed O_3 fluxes and $v_d(O_3)$ values far more accurately than does GC alone (Figure 3). The $v_d(O_3)$ values observed during FluCS and C19 are captured by MLC/GC to within 8%, on average, and all simulated flux and $v_d(O_3)$ diel profiles more closely match the observationally constrained MLC output—showing that surface-atmosphere exchange processes are more appropriately represented in MLC/GC than in GC alone. The modeled fluxes and $v_d(O_3)$ values exhibit only slightly less predictive skill on a day-to-day basis than those from MLC (Figure 4), and (like MLC) the daytime-mean $v_d(O_3)$ values predicted by MLC/GC at FluCS and C19 depend strongly on VPD and RH ($r^2 \sim 0.60$). Discrepancies that do exist between the MLC and MLC/GC predictions arise primarily from differences in the meteorological inputs that govern g_s and g_{ns}; this point is discussed further in Section 3.4.

To test whether the predictive improvements in MLC/GC relative to GC arise mainly from the resolved canopy or from the updated parameterization of the dry deposition process itself, we repeated the MLC/GC simulations using the W89 (as in GC) rather than A-g_s representation of stomatal conductance. We find using this implementation that the deposition overestimates seen in GC are exacerbated, with $v_d(O_3)$ predictions 1.3× higher than the GC estimates and up to 2.1× higher than the observations (Figure S6 in Supporting Information S1). This degradation is primarily due to a poor representation of g_s in W89 and shows that there are compensating errors between the W89 parameterization and the big-leaf canopy treatment. A model such as GC that uses both will likely be unable to resolve the true patterns of deposition variability due to this misrepresentation of the underlying physical and biological dependencies. The MLC/GC O_3 deposition improvement thus results from the combination of (a) more representative stomatal/nonstomatal parameterizations and (b) an explicit vertically dynamic canopy environment. We show in Section 3.6 that the latter is required to explain the (vertically dependent) flux partitioning as a function of underlying loss process (i.e., stomatal, nonstomatal, and in-canopy chemistry) and across model layers where environmental drivers can change.

Furthermore, the inclusion of a vertically resolved canopy enables a representation of concentration gradients that is otherwise missing from CTMs. This capability manifests in the strong day/night variation in $[O_3]_{canopy}$ that is simulated by MLC/GC, which arises from a more realistic treatment of nocturnal vertical transport to the canopy.

For example, although the surface O_3 concentrations predicted by GC for FluCS only vary by an average of 2.6 ppb between day and night, the in-canopy O_3 concentrations simulated by MLC/GC vary by 12 ppb—in close agreement with observations (14 ppb) (Figure 3). The absence of near-surface vertical transport in CTMs thus translates to an incorrect representation of ground-level pollutant concentrations, underscoring the importance of extending the atmospheric column in CTMs below the surface layer. Inclusion of additional model surface layers would also benefit [O_3] predictions beyond the forest canopy and would help to reduce CTM representation errors arising from O_3 gradients in the lower atmosphere (Makar et al., 2017; Travis et al., 2016).

Across all runs, we see that the in-canopy O_3 concentrations predicted by MLC/GC are higher than in MLC (and higher than the observations) because of the positive surface O_3 bias in the parent GC model (Figure 3). Since GC also overestimates $v_d(O_3)$ over the examined ecosystems (by ~40% on average), we might expect the GC surface O_3 bias to be exacerbated over these regions in a fully online regional or global MLC/GC implementation. If so, this could reflect some offsetting error in another part of the CTM; however, definitive assessment will require moving beyond the offline approach used here to an online, two-way coupled MLC/GC capability. Regardless, based on the analyses above, we conclude that for these ecosystems MLC/GC provides a significant improvement in the process-level representation of near-surface O_3 over current CTM implementations.

3.4. Relative Humidity and Solar Irradiance Are Key Drivers of Remaining O_3 Deposition Biases

Prediction biases that do occur in MLC/GC are primarily due to errors in the GEOS-FP meteorological fields. In particular, the mismatch in the daytime $v_d(O_3)$ peak between MLC and MLC/GC seen in Figure 3 is largely removed when using observed rather than GEOS-FP solar radiation, RH, and T fields to constrain MLC/GC (Figure S8 in Supporting Information S1). This $v_d(O_3)$ improvement arises mainly from a more realistic representation of solar radiation (which controls g_s) during the daytime and of RH (which controls nocturnal cuticle uptake) at night: agreement between MLC and MLC/GC thus improves significantly when MLC/GC is constrained with RH and solar radiation observations (Figures S8a–S8d in Supporting Information S1). Meteorological uncertainties also affect the MLC/GC representation of VPD (and thus g_s), and better model performance is likewise obtained when constraining RH and T (Figures S8e–S8h). In the case of FluCS, the GEOS-FP solar radiation bias leads to a $v_d(O_3)$ overestimate unless the radiation observations are also ingested (Figures S8i–S8l in Supporting Information S1).

Constraining MLC/GC with K_H observations rather than with the GEOS-FP level-1 values has little effect on the daytime $v_d(O_3)$ predictions, with some impact at night through increased nocturnal turbulence and therefore $v_d(O_3)$ (e.g., during FluCS; Figures S8m–S8p in Supporting Information S1). This finding, along with the good model-measurement agreement for $v_d(O_3)$ across sites, generally supports the first-order closure assumptions in MLC, validates the inference of in-canopy K_H values from the GEOS-FP layer-1 quantities, and implies active daytime coupling between the above-canopy and in-canopy air volumes for the sites in this study. This does not always hold in more closed canopies as shown previously for a dense deciduous forest where $v_d(O_3)$ was overestimated by MLC-CHEM during decoupling periods (Visser et al., 2022). Decoupling conditions were encountered on 23% of the evenings during PROPHET-AMOS (Wei et al., 2020). However, this reduced mixing did not notably affect the mean $v_d(O_3)$ or [O_3]$_{canopy}$ behavior during the study partially due to the low nocturnal $v_d(O_3)$ values. Overall, a CTM with a resolved canopy based on MLC-CHEM will be well suited for predicting regional lifetimes against deposition, particularly if it incorporates an improved treatment of vertical transport that accounts for decoupled conditions.

3.5. Nonstomatal Loss Is a Major Component of O_3 Deposition, but In-Canopy Chemistry Is Not

The fact that MLC is able to capture the magnitude and much of the variability in the observed O_3 fluxes and $v_d(O_3)$ values indicates that we can employ this model to identify the main processes contributing to O_3 deposition at these sites. To do so, we rearrange Equation 2 to express the above-canopy turbulent vertical flux as the integral of dry deposition, chemistry, and air storage throughout the canopy (layers $l = 1,2$) and below the EC sensors (Figure 1). The diel contributions for each of these terms are then plotted in Figure 5 for MLC with dry deposition further partitioned into stomatal and nonstomatal components. Additional plots in Supporting Information S1 show the mean concentration tendencies ($\frac{\partial [O_3]_l}{\partial t}$) (Figure S9 in Supporting Information S1) and normalized tendencies ($\frac{1}{[O_3]_l}\frac{\partial [O_3]_l}{\partial t}$) for each site (Figure S10 in Supporting Information S1).
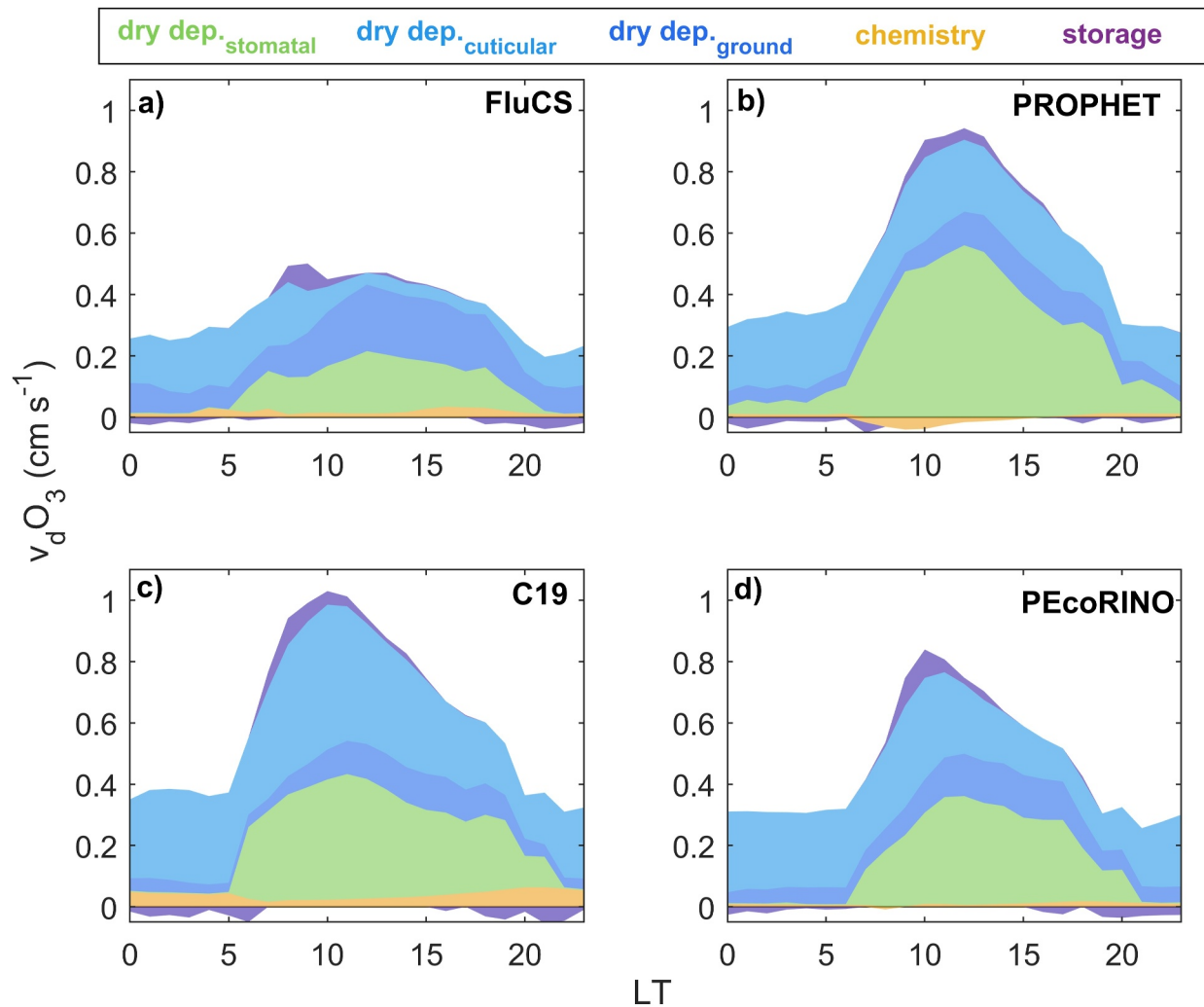
Figure 5. Processes contributing to O$_3$ deposition during four field studies as computed by MLC. The mean diel contributions of stomatal dry deposition, nonstomatal dry deposition (to cuticles and the ground), in-canopy chemistry, and air storage to the total O$_3$ deposition velocities are shown for (a) FluCS, (b) PROPHET, (c) C19, and (d) PEcoRINO.

Figure 5 shows that dry deposition provides the vast majority of the total O$_3$ flux at all sites. In most cases, this loss occurs mainly in the upper canopy (Figures S9–S10 in Supporting Information S1); an exception is FluCS, which featured the lowest LAI and highest $K_{H,cl}$ values among all of the studies—enabling more efficient exchange with the lower canopy and ground. This process would not be resolved in big-leaf representations of deposition, which do not enable any vertical flux attribution. We find that stomatal uptake accounts for 27%–45% of the campaign-mean O$_3$ flux across the studies in line with findings from other north temperate forests (Clifton et al., 2023; Fares et al., 2010; Neirynck et al., 2012; Visser et al., 2021). In general, this depositional pathway peaks during late morning and shuts off at night (Figure 5). Nonstomatal O$_3$ losses (to plant cuticles and the ground) are larger than the stomatal losses during all four studies and represent 52%–66% of the campaign-mean fluxes—with campaign-mean ranges of 0.24–0.37 cm s^{-1} and −11−−6.5 nmol m^{-2} s^{-1} for the nonstomatal v_d(O$_3$) values and O$_3$ fluxes, respectively. Sustained nighttime nonstomatal loss is predicted by MLC at all sites (Figure 5); observations during FluCS suggest that this nocturnal pathway is overestimated by the model (Figure 3 and Section 3.1), but this does not have a large impact on the overall O$_3$ budget since flux magnitudes are low at this time. The above dry deposition partitioning changes significantly if we instead use the W89 parameterization that is widely employed in CTMs. In particular, W89 strongly underestimates the nonstomatal fraction of dry deposition velocities (21%–30% vs. 55%–59%; Figure S11 in Supporting Information S1) due to lower g_{ns} and higher g_s. This finding is

consistent with that of Visser et al. (2021) and has important implications for proper estimation of surface toxicity effects (described further in 3.6).

Nonstomatal fluxes are dominated by cuticular uptake (68%–80% of campaign means; Figure 5) for all cases except FluCS (40%) with its sparser canopy. Ground O_3 uptake is limited by in-canopy turbulence (r_{ac}; Equation 6), and its fractional contribution to the total nonstomatal flux therefore increases during the day to ~75% during FluCS and 25%–40% for the other studies. Leaf-level O_3 uptake measurements during PROPHET revealed high variability between tree species with high nonstomatal deposition to white pine needles ($v_d(O_3) \sim 0.30$ cm s^{-1}; 75% of total $v_d(O_3)$ during evening) but no detectable cuticular uptake for broadleaf species (red maple, bigtooth aspen, and red maple) (Wang et al., 2020). However, those findings were based on only 2 days of measurements.

Chemical loss to reactive terpenes and NO is a minor contributor to the total MLC-computed O_3 uptake for all studies, accounting for ≤7% of total removal (Table S4 in Supporting Information S1). This is comparable to previously published estimates of the in-canopy chemistry fraction (2%–4%) all in pine-dominated ecosystems (Wolfe et al., 2011; Zhou et al., 2017). Chemical O_3 removal is strongest in the early morning and late evening (Figure 5, Figure S9–S10 in Supporting Information S1) primarily due to VOC ozonolysis, and its fractional contribution is higher at this time (e.g., 14% for C19) when stomatal loss is also low. The chemical O_3 loss derived here for C19 (up to 0.15 cm s^{-1}) is lower than was previously inferred for the same field study (up to 0.70 cm s^{-1}; Vermeuel et al., 2021) based on the difference between the observed O_3 flux and an estimated stomatal component. Although the summed nonstomatal dry deposition and chemical loss obtained here agrees with the Vermeuel et al. (2021) result to within 7%, the updated dry deposition parameterization employed here eliminates most of the unexplained residual that was attributed previously to chemistry.

For all simulations, reactions with SQT provide the primary in-canopy chemical loss with MT of minor importance. When we replace the default k_{MT+O3} value in MLC (based on α-pinene, which has the median rate across observed MT) with the rate coefficient for our most reactive observed MT (β-ocimene), the total chemical O_3 loss increases by just 1% in the 24-hr mean and by 2% at night. The net in-canopy chemical tendencies for O_3 were negative (i.e., removal) for all studies except PROPHET with the PEcoRINO simulation exhibiting a modest positive tendency during the morning (~7–8 LT; Figure S9o in Supporting Information S1) when NO_x was sufficiently high to drive net O_3 production. For PROPHET, in-canopy isoprene concentrations were high enough (averaging 6.3 ppb in MLC) to sustain net daytime O_3 production and provide a small offset to daytime deposition. This shows that in-canopy O_3 production can also occur on turbulent timescales and affect observed fluxes.

Prior analyses support the idea that MLC treatment used here captures the gas-phase chemistry controlling in-canopy O_3 production/loss, so that the associated contribution to deposition is indeed low at these sites. In particular, assessments of the comprehensive chemical observations from PROPHET-AMOS and FluCS concluded that the total OH and O_3 reactivity at these sites is controlled by species treated explicitly in the model mechanisms employed here—rather than by missing or unrepresented compounds. For example, Millet et al. (2018) found that 95% of the OH reactivity flux at PROPHET-AMOS was from known and modeled compounds, whereas Vermeuel, Millet, et al. (2023) report that MT, SQT, 232-MBO, and isoprene alone made up 85% of the total O_3 reactivity flux at FluCS-2021. The VOC emission profile at US-PFa (C19/PEcoRINO) is broadly similar to that at PROPHET-AMOS and we therefore expect the dominant reactivity drivers to also be similar.

We find that storage ($\int_{l=1}^{l=2} \frac{\partial [O_3]_l}{\partial t} dz$) is the smallest $v_d(O_3)$ component, comprising up to 3% of the total. At all sites, low turbulence and stable nocturnal stratification causes a net drawdown of the in-canopy O_3 column as nonstomatal loss continues through the night. During the transition from the nocturnal to daytime boundary layer (~8–10 LT), mixing is increased and more O_3 enters the canopy than is removed—leading to net accumulation. This night-to-day vertical mixing transition was previously observed during FluCS to affect 232-MBO (Vermeuel, Millet, et al., 2023), which likewise had a small but nonzero storage term.

The O_3 flux breakdown derived above on the basis of MLC is very similar if we instead employ MLC/GC (Figure S12 in Supporting Information S1). Differences arise from the use of GEOS-FP rather than observed RH, PPFD and u_* values, which leads to slight changes in the mean stomatal fraction (35% in MLC/GC vs. 34% in MLC) and increases the importance of ground uptake in the case of FluCS (70% of nonstomatal loss in MLC/GC vs. 60% in MLC). The in-canopy chemistry contribution decreases when using MLC/GC (to ≤3%) primarily because the

relevant VOC emission factors are underestimated in GEOS-Chem. Nevertheless, the overall $v_d(O_3)$ magnitudes, the underlying process contributions, and their relative importance are highly consistent between the observationally constrained best estimates provided by MLC and the GEOS-FP constrained values from MLC/GC—supporting the use of MLC/GC in a fully online implementation for north temperate forest ecosystems. Since the field data sets analyzed here are geographically limited, further MLC/GC evaluation across other ecosystems would help in assessing its broader suitability in this regard.

3.6. A Resolved-Canopy Implementation With Updated Dry Deposition Parameterizations Greatly Improves Estimates of Phytotoxicity

The improved process representation of O_3 deposition provided by MLC/GC enables more accurate CTM predictions of ecological O_3 impacts. The cumulative stomatal uptake of O_3 (CUO; mmol m^{-2}) (Karlsson et al., 2004) is the leading physiological metric for plant O_3 damage and is used in global Earth system models to forecast the resulting effects on carbon and water cycling (Arnold et al., 2018; Clifton et al., 2020; Lombardozzi et al., 2015). Effective doses for adverse O_3 effects on vegetation are derived from CUO calculations that sum stomatal fluxes above a detoxification threshold Y in nmol (m^2 PLA)$^{-1}$ s^{-1}, where PLA is the one-sided projected leaf area to obtain a phytotoxic ozone dose (POD_Y) over a growing season of n days. A Y value of 1 nmol (m^2 PLA)$^{-1}$ s^{-1} is commonly employed for forest trees (Anav et al., 2016; Eghdami et al., 2022; Finco et al., 2017; Marzuoli et al., 2018; Mills et al., 2011; Neirynck et al., 2012), so that:

$$POD_1 = 10^6 \int_{t=0}^{t=n} \max \left(\frac{F(O_3)_{stomatal}}{LAI} - 1 \, \frac{nmol}{(m^2 \, PLA)(s)}, 0 \right) dt \tag{7}$$

POD_1 is then used in response functions to predict relative biomass yields (RY) for crops, forest trees, and other vegetation (Mills et al., 2011). In the calculation above, we divide $F(O_3)_{stomatal}$ by LAI to obtain fluxes per leaf area rather than per ground area.

Figure 6 compares the time-varying POD_1 values derived for our four field studies via Penman-Monteith (PM) inversion (Monteith, 1965; Shuttleworth et al., 1984; Supporting Information S3) and via the MLC, MLC/GC, and GC simulations. We also compute a cumulative growing-season $POD_{1,season}$ value for each site by extending a linear fit of POD_1 versus time ($r^2 \geq 0.97$) through a nominal growing-season length of 153 days (15 April to 15 September). Although changing leaf phenology means that these fits may not perfectly capture the early and late growing season outside of our measurement period, we expect the relative differences between the above estimates to be robust. We employ the resulting $POD_{1,season}$ values to then obtain simplified seasonal RY estimates for deciduous (as beech or birch) and coniferous (as Norway spruce) trees (Mills et al., 2011).

We see in Figure 6 that the MLC $POD_{1,season}$ values range from 4.8 to 10 mmol (m^2 PLA)$^{-1}$ across our sites in good agreement with the observationally based PM estimates. These values fall near the low end of published estimates derived from flux observations over multiple temperate forests in different years (7.1–22 mmol (m^2 PLA)$^{-1}$) (Gerosa et al., 2022; Neirynck et al., 2012), reflecting the lower daytime $[O_3]_{surface}$ values at our sites (23–50 vs. 45–70 ppb). Meanwhile, the GC big-leaf treatment strongly overestimates ozone damage across the ecosystems examined here—with $POD_{1,season}$ overpredicted by up to 6.9× and RY reductions overestimated by up to 1.5× relative to both PM and MLC. The MLC/GC values also exhibit some high bias due to their reliance on GC $[O_3]_{surface}$ (which is overestimated), but the MLC/GC $POD_{1,season}$ predictions are nevertheless 2.6× lower than GC and in better agreement with the PM-derived POD estimates due to the more physical representation of g_s, g_{ns}, and canopy structure.

Here, the relatively short observational data sets analyzed prevent any assessment of interannual variability. Regional stomatal uptake of O_3 can vary significantly through time with one study finding POD_1 changes of up to 2.1× between years at a single site (Gerosa et al., 2022), and another study reporting high CUO variability (CVs exceeding 20%) across different global regions throughout the 2010s (Clifton et al., 2020). This interannual variability may arise from climactic and ecological factors (e.g., light, rainfall, phenology) that influence CO_2 assimilation (Baldocchi et al., 2018) along with less-studied mechanisms including the impact of O_3 damage on the assimilation:transpiration ratio. Additional studies leveraging long term O_3 flux data sets (e.g., Clifton et al., 2017; Fares et al., 2010; Visser et al., 2021) are needed to explore such mechanisms and to extend the analyses here to longer timeframes.
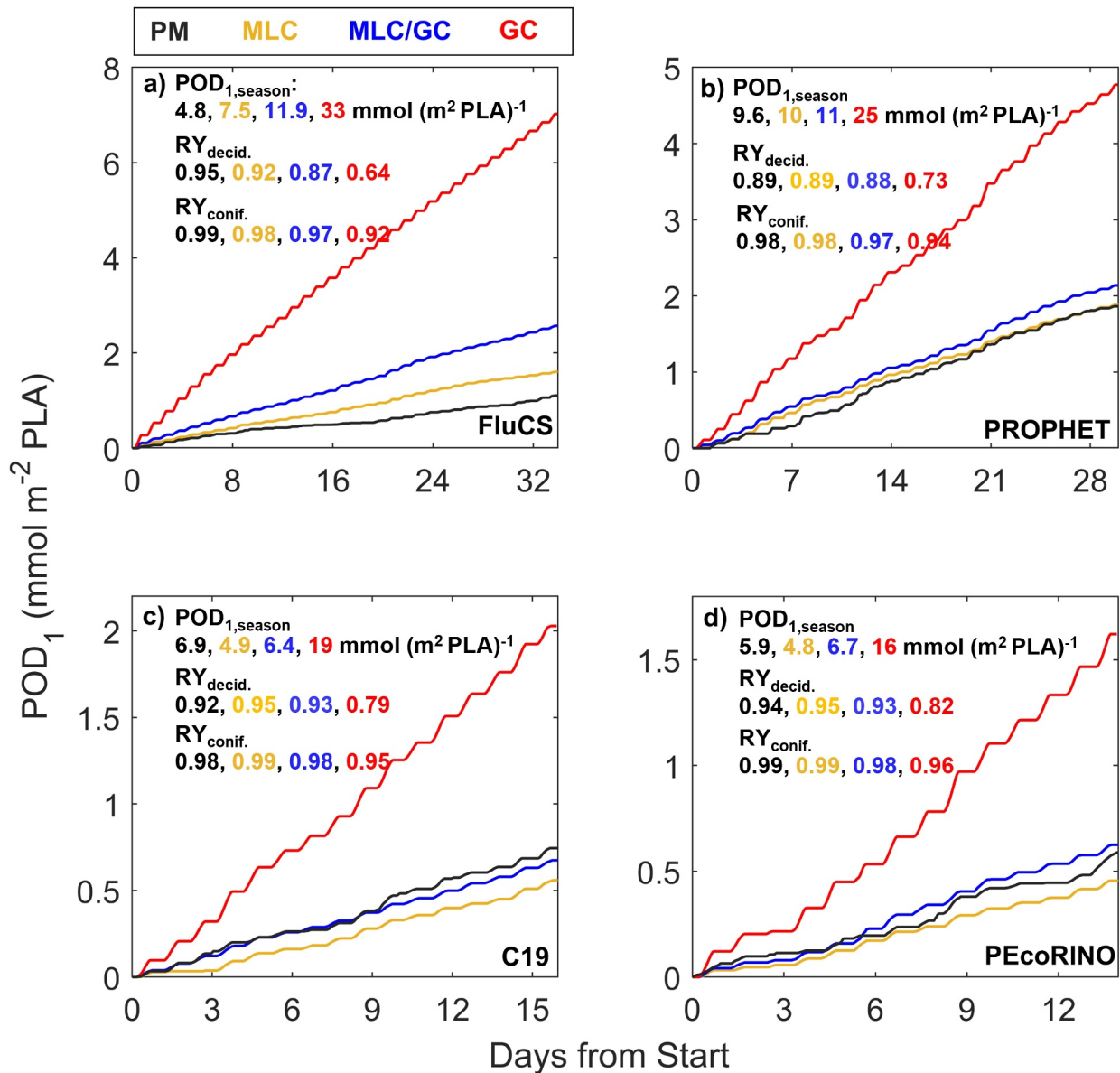
Figure 6. Phytotoxic ozone dose above a threshold of 1 nmol $(m^2\ PLA)^{-1}\ s^{-1}$ (POD_1) for four field studies. Results plotted are computed based on Penman-Monteith (PM) inversion (black) or from the MLC (gold), MLC/GC (blue), and GEOS-Chem (red) simulations. Listed inset are the POD_1 values scaled to the growing season ($POD_{1,season}$) and the relative yields (RY) for deciduous and coniferous biomass.

4. Conclusions

Current CTM deposition schemes provide an overly simplistic representation of surface-atmosphere exchange, limiting our ability to predict O_3 uptake and near-surface concentrations. Here, we showed that a vertically resolved canopy that considers turbulence, dry deposition, and chemistry within canopy layers, implemented with more physiologically appropriate dry deposition parameterizations, enables more accurate O_3 deposition estimates across three north temperate forests. We find that GEOS-Chem (GC) O_3 flux and $v_d(O_3)$ estimates are consistently higher than those calculated from the MLC-CHEM (MLC) vertical canopy model, and the GC O_3 fluxes are also up to 2× higher than the observed values. The O_3 flux bias in GC arises from overestimates in both $[O_3]_{surface}$ and $v_d(O_3)$ with the latter up to 1.5× larger than observed. The MLC runs largely reproduce the observed $v_d(O_3)$ diel profiles, particularly during daytime, validating the MLC-CHEM representation of non-stomatal removal mechanisms and the A-g_s model for representing stomatal loss. One exception occurred during

FluCS, where $v_d(O_3)$ was overestimated at night, pointing to a need for improved representation of f_{wet} and of reactive O_3 uptake to wet needle leaves and ground surfaces.

Incorporating the MLC resolved canopy within GC (MLC/GC) yields O_3 flux and $v_d(O_3)$ predictions that substantially outperform those from GC alone, thus offering a potential pathway to improved simulation of near-surface $[O_3]$. Day-to-day variability in the observed O_3 fluxes and $v_d(O_3)$ values was most associated with VPD, RH, and solar radiation, and we were able to capture half or more of this variability with MLC and MLC/GC—albeit with a stronger parameterized dependence on these meteorological drivers than was observed. By contrast, O_3 deposition variability in GC was primarily driven by u_* and LAI. The MLC and MLC/GC $[O_3]_{canopy}$ predictions provide a better representation of ground-level O_3 than is possible with GC due to their treatment of vertical exchange between the surface and canopy layers and more realistic dry deposition parameterizations. Remaining biases in MLC/GC arise mainly from uncertainties in the GEOS-FP meteorological fields—in particular for RH and solar radiation, which control predictions of nonstomatal uptake on wet surfaces and stomatal loss.

Fluxes from all four field studies were dominated by nonstomatal dry deposition (averaging 60% of the total). In-canopy chemistry was a small fraction of the MLC/GC deposition ($\leq 7\%$ for 24-hr mean) consistent with findings from other canopy-model studies, whereas air storage was negligible when averaged over the day. We showed that phytotoxicity arising from stomatal O_3 uptake (calculated as POD_1) is overpredicted by as much as $\sim 7\times$ when using CTM deposition schemes, which translates to a $1.5\times$ overestimate of biomass yield reductions for forest trees. Our analyses are based on 35 days (at most) of data and do not assess how well MLC/GC captures patterns and drivers of interannual variability; prior work has shown that these are not well-resolved by current CTMs (Wong et al., 2022). One recent multiyear comparison found that summertime interannual variability in O_3 fluxes was well-represented by MLC-CHEM relative to other schemes (Clifton et al., 2023), lending support to a CTM implementation for long-term analyses.

This work motivates the incorporation of a vertically resolved canopy and up-to-date dry deposition parameterizations within CTMs to improve predictions of atmospheric O_3 and its impacts on terrestrial ecosystems. Some issues should be addressed prior to a global implementation. In particular, our study is based on observations over three midlatitude forests, and assessment over a wider range of ecosystems is needed. An additional consideration is the tradeoff between added model complexity and model speed. However, MLC-CHEM has been previously applied online in a chemistry-climate model for simulating in-canopy transport and chemistry (Ganzeveld et al., 2002a, 2010), and we estimate that an online implementation in GEOS-Chem using two canopy layers would increase model runtimes by just $\sim 5\%$. In addition to O_3, a fully online global framework of this type would improve model representation of surface-atmosphere exchange for other soluble and reactive compounds. This includes oxygenated VOCs that represent the majority of the reactive carbon pool (Chen et al., 2019; Safieddine et al., 2017) and influence secondary organic aerosol formation (Hallquist et al., 2009; Jimenez et al., 2009) and very reactive VOCs such as SQT that have chemical lifetimes on the order of canopy turbulent timescales and can affect in-canopy oxidation.

Data Availability Statement

Observational data, GEOS-Chem input files, and MLC-CHEM code for the MLC and MLC/GC runs presented here can be accessed at the Data Repository for the University of Minnesota (Vermeuel et al., 2024) The model code for GEOS-Chem v13.3 can be accessed at a publicly available repository (The International GEOS-Chem User Community, 2021).

References

Ainsworth, E. A., Yendrek, C. R., Sitch, S., Collins, W. J., & Emberson, L. D. (2012). The effects of tropospheric ozone on net primary productivity and implications for climate change. *Annual Review of Plant Biology*, *63*(1), 637–661. https://doi.org/10.1146/annurev-arplant-042110-103829

Altimir, N., Kolari, P., Tuovinen, J.-P., Vesala, T., Bäck, J., Suni, T., et al. (2006). Foliage surface ozone deposition: A role for surface moisture? *Biogeosciences*, *3*(2), 209–228. https://doi.org/10.5194/bg-3-209-2006

Alwe, H. D., Millet, D. B., Chen, X., Raff, J. D., Payne, Z. C., & Fledderman, K. (2019). Oxidation of volatile organic compounds as the major source of formic acid in a mixed forest canopy. *Geophysical Research Letters*, *46*(5), 2940–2948. https://doi.org/10.1029/2018GL081526

Anav, A., De Marco, A., Proietti, C., Alessandri, A., Dell'Aquila, A., Cionni, I., et al. (2016). Comparing concentration-based (AOT40) and stomatal uptake (PODY) metrics for ozone risk assessment to European forests. *Global Change Biology*, *22*(4), 1608–1627. https://doi.org/10.1111/gcb.13138

Arnold, S. R., Lombardozzi, D., Lamarque, J. F., Richardson, T., Emmons, L. K., Tilmes, S., et al. (2018). Simulated global climate response to tropospheric ozone-induced changes in plant transpiration. *Geophysical Research Letters*, *45*(23), 13070–13079. https://doi.org/10.1029/2018GL079938

Ashworth, K., Chung, S. H., Griffin, R. J., Chen, J., Forkel, R., Bryan, A. M., & Steiner, A. L. (2015). Forest canopy atmosphere transfer (FORCAsT) 1.0: A 1-D model of biosphere-atmosphere chemical exchange. *Geoscientific Model Development*, *8*(11), 3765–3784. https://doi.org/10.5194/gmd-8-3765-2015

Atkinson, R., & Arey, J. (2003). Gas-phase tropospheric chemistry of biogenic volatile organic compounds: A review. *Atmospheric Environment*, *37*, 197–219. https://doi.org/10.1016/S1352-2310(03)00391-1

Avnery, S., Mauzerall, D. L., Liu, J., & Horowitz, L. W. (2011). Global crop yield reductions due to surface ozone exposure: 2. Year 2030 potential crop production losses and economic damage under two scenarios of O_3 pollution. *Atmospheric Environment*, *45*(13), 2297–2309. https://doi.org/10.1016/j.atmosenv.2011.01.002

Baldocchi, D., Chu, H., & Reichstein, M. (2018). Inter-annual variability of net and gross ecosystem carbon fluxes: A review. *Agricultural and Forest Meteorology*, *249*, 520–533. https://doi.org/10.1016/j.agrformet.2017.05.015

Baldocchi, D. D., Hicks, B. B., & Camara, P. (1987). A canopy stomatal resistance model for gaseous deposition to vegetated surfaces. *Atmospheric Environment*, *21*(1), 91–101. https://doi.org/10.1016/0004-6981(87)90274-5

Bates, K. H., & Jacob, D. J. (2019). A new model mechanism for atmospheric oxidation of isoprene: Global effects on oxidants, nitrogen oxides, organic products, and secondary organic aerosol. *Atmospheric Chemistry and Physics*, *19*(14), 9613–9640. https://doi.org/10.5194/ACP-19-9613-2019

Bates, K. H., Jacob, D. J., Wang, S., Hornbrook, R. S., Apel, E. C., Kim, M. J., et al. (2021). The global budget of atmospheric methanol: New constraints on secondary, oceanic, and terrestrial sources. *Journal of Geophysical Research: Atmospheres*, *126*(4), e2020JD033439. https://doi.org/10.1029/2020JD033439

Bhujel, M., Marshall, D. L., Maccarone, A. T., McKinnon, B. I., Trevitt, A. J., da Silva, G., et al. (2020). Gas phase reactions of iodide and bromide anions with ozone: Evidence for stepwise and reversible reactions. *Physical Chemistry Chemical Physics*, *22*(18), 9982–9989. https://doi.org/10.1039/d0cp01498b

Bryan, A. M., Bertman, S. B., Carroll, M. A., Dusanter, S., Edwards, G. D., Forkel, R., et al. (2012). In-canopy gas-phase chemistry during CABINEX 2009: Sensitivity of a 1-D canopy model to vertical mixing and isoprene chemistry. *Atmospheric Chemistry and Physics*, *12*(18), 8829–8849. https://doi.org/10.5194/acp-12-8829-2012

Bui, A. A. T., Wallace, H. W., Kavassalis, S., Alwe, H. D., Flynn, J. H., Erickson, M. H., et al. (2021). Transport-driven aerosol differences above and below the canopy of a mixed deciduous forest. *Atmospheric Chemistry and Physics*, *21*(22), 17031–17050. https://doi.org/10.5194/acp-21-17031-2021

Butterworth, B. J., Desai, A. R., Metzger, S., Townsend, P. A., Schwartz, M. D., Petty, G. W., et al. (2021). Connecting land–atmosphere interactions to surface heterogeneity in CHEESEHEAD19. *Bulletin America Meteorology Social*, *102*(2), E421–E445. https://doi.org/10.1175/BAMS-D-19-0346.1

Chen, X., Millet, D. B., Singh, H. B., Wisthaler, A., Apel, E. C., Atlas, E. L., et al. (2019). On the sources and sinks of atmospheric VOCs: An integrated analysis of recent aircraft campaigns over north America. *Atmospheric Chemistry and Physics*, *19*(14), 9097–9123. https://doi.org/10.5194/acp-19-9097-2019

Cionco, R. M. (1972). A wind-profile index for canopy flow. *Boundary-Layer Meteorology*, *3*(2), 255–263. https://doi.org/10.1007/BF02033923

Claflin, M. S., Pagonis, D., Finewax, Z., Handschy, A. V., Day, D. A., Brown, W. L., et al. (2021). An in situ gas chromatograph with automatic detector switching between PTR- and EI-TOF-MS: Isomer-resolved measurements of indoor air. *Atmospheric Measurement Techniques*, *14*(1), 133–152. https://doi.org/10.5194/amt-14-133-2021

Clifton, O. E., Fiore, A. M., Munger, J. W., Malyshev, S., Horowitz, L. W., Shevliakova, E., et al. (2017). Interannual variability in ozone removal by a temperate deciduous forest. *Geophysical Research Letters*, *44*(1), 542–552. https://doi.org/10.1002/2016GL070923

Clifton, O. E., Lombardozzi, D. L., Fiore, A. M., Paulot, F., & Horowitz, L. W. (2020). Stomatal conductance influences interannual variability and long-term changes in regional cumulative plant uptake of ozone. *Environmental Research Letters*, *15*(11), 114059. https://doi.org/10.1088/1748-9326/abc3f1

Clifton, O. E., Schwede, D., Hogrefe, C., Bash, J. O., Bland, S., Cheung, P., et al. (2023). A single-point modeling approach for the intercomparison and evaluation of ozone dry deposition across chemical transport models (Activity 2 of AQMEII4). *Atmospheric Chemistry and Physics*, *23*(17), 9911–9961. https://doi.org/10.5194/acp-23-9911-2023

Davis, K. J., Bakwin, P. S., Yi, C., Berger, B. W., Zhao, C., Teclaw, R. M., & Isebrands, J. G. (2003). The annual cycles of CO2 and H2O exchange over a northern mixed forest as observed from a very tall tower. *Global Change Biology*, *9*, 1278–1293. https://doi.org/10.1046/j.1365-2486.2003.00672.x

Delang, M. N., Becker, J. S., Chang, K. L., Serre, M. L., Cooper, O. R., Schultz, M. G., et al. (2021). Mapping yearly fine resolution global surface ozone through the Bayesian maximum entropy data fusion of observations and model output for 1990-2017. *Environmental Science and Technology*, *55*(8), 4389–4398. https://doi.org/10.1021/acs.est.0c07742

Desai, A. R. (1996). AmeriFlux US-PFa Park falls/WLEF. https://doi.org/10.17190/AMF/1246090

Dörich, R., Eger, P., Lelieveld, J., & Crowley, J. N. (2021). Iodide CIMS and m/z 62: The detection of HNO_3 as NO_3^- in the presence of PAN, peroxyacetic acid and ozone. *Atmospheric Measurement Techniques*, *14*(8), 5319–5332. https://doi.org/10.5194/amt-14-5319-2021

Eghdami, H., Werner, W., Büker, P., & Sicard, P. (2022). Assessment of ozone risk to Central European forests: Time series indicates perennial exceedance of ozone critical levels. *Environmental Research*, *203*, 111798. https://doi.org/10.1016/j.envres.2021.111798

El-Madany, T. S., Niklasch, K., & Klemm, O. (2017). Stomatal and non-stomatal turbulent deposition flux of ozone to a managed peatland. *Atmosphere*, *8*(9), 1–16. https://doi.org/10.3390/atmos8090175

Fantechi, G., Jensen, N. R., Hjorth, J., & Peeters, J. (1998). Mechanistic studies of the atmospheric oxidation of methyl butenol by OH radicals, ozone and NO_3 radicals. *Atmospheric Environment*, *32*(20), 3547–3556. https://doi.org/10.1016/S1352-2310(98)00061-2

Fares, S., McKay, M., Holzinger, R., & Goldstein, A. H. (2010). Ozone fluxes in a Pinus ponderosa ecosystem are dominated by non-stomatal processes: Evidence from long-term continuous measurements. *Agricultural and Forest Meteorology*, *150*(3), 420–431. https://doi.org/10.1016/j.agrformet.2010.01.007

Finco, A., Marzuoli, R., Chiesa, M., & Gerosa, G. (2017). Ozone risk assessment for an Alpine larch forest in two vegetative seasons with different approaches: Comparison of POD1 and AOT40. *Environmental Science & Pollution Research*, *24*(34), 26238–26248. https://doi.org/10.1007/s11356-017-9301-1

Fisher, J. A., Atlas, E. L., Barletta, B., Meinardi, S., Blake, D. R., Thompson, C. R., et al. (2018). Methyl, ethyl, and propyl nitrates: Global distribution and impacts on reactive nitrogen in remote marine environments. *Journal of Geophysical Research: Atmospheres*, *123*(21), 12429–12451. https://doi.org/10.1029/2018JD029046

Foken, T., & Wichura, B. (1996). Tools for quality assessment of surface-based flux measurements. *Agricultural and Forest Meteorology*, *78*(1–2), 83–105. https://doi.org/10.1016/0168-1923(95)02248-1

Ganzeveld, L., Bouwman, L., Stehfest, E., Van Vuuren, D. P., Eickhout, B., & Lelieveld, J. (2010). Impact of future land use and land cover changes on atmospheric chemistry-climate interactions. *Journal of Geophysical Research*, *115*(D23), 1–18. https://doi.org/10.1029/2010JD014041

Ganzeveld, L., & Lelieveld, J. (1995). Dry deposition parameterization in a chemistry general circulation model and its influence on the distribution of reactive trace gases. *Journal of Geophysical Research*, *100*(D10), 20999–21012. https://doi.org/10.1029/95jd02266

Ganzeveld, L., Lelieveld, J., & Roelofs, G. J. (1998). A dry deposition parameterization for sulfur oxides in a chemistry and general circulation model. *Journal of Geophysical Research*, *103*(D5), 5679–5694. https://doi.org/10.1029/97JD03077

Ganzeveld, L. N., Lelieveld, J., Dentener, F. J., Krol, M. C., Bouwman, A. J., & Roelofs, G. J. (2002c). Global soil-biogenic NO_x emissions and the role of canopy processes. *Journal of Geophysical Research*, *107*(ACH 9–1-ACH 9–17). https://doi.org/10.1029/2001JD001289

Ganzeveld, L. N., Lelieveld, J., Dentener, F. J., Krol, M. C., & Roelofs, G. J. (2002a). Atmosphere-biosphere trace gas exchanges simulated with a single-column model. *Journal of Geophysical Research*, *107*(D16), 1–21. https://doi.org/10.1029/2001jd000684

Ganzeveld, L. N., Lelieveld, J., Dentener, F. J., Krol, M. C., & Roelofs, G.-J. (2002b). Atmosphere-biosphere trace gas exchanges simulated with a single-column model. *Journal of Geophysical Research*, *107*(D16), 1–21. https://doi.org/10.1029/2001JD000684

Gerosa, G. A., Marzuoli, R., & Finco, A. (2022). Interannual variability of ozone fluxes in a broadleaf deciduous forest in Italy. *Elementa*, *10*, 1–22. https://doi.org/10.1525/elementa.2021.00105

Giglio, L., Randerson, J. T., & Van Der Werf, G. R. (2013). Analysis of daily, monthly, and annual burned area using the fourth-generation global fire emissions database (GFED4). *Journal of Geophysical Research: Biogeosciences*, *118*(1), 317–328. https://doi.org/10.1002/JGRG.20042

Goldstein, A. H., McKay, M., Kurpius, M. R., Schade, G. W., Lee, A., Holzinger, R., & Rasmussen, R. A. (2004). Forest thinning experiment confirms ozone deposition to forest canopy is dominated by reaction with biogenic VOCs. *Geophysical Research Letters*, *31*(22), 1–4. https://doi.org/10.1029/2004GL021259

Gough, C., Bohrer, G., & Curtis, P. (2023). AmeriFlux BASE US-UMB Univ. Of Mich. Biological station, ver. *AmeriFlux AMP, (Dataset)*, *20*–5. https://doi.org/10.17190/AMF/1246107

Gough, C. M., Hardiman, B. S., Nave, L. E., Bohrer, G., Maurer, K. D., Vogel, C. S., et al. (2013). Sustained carbon uptake and storage following moderate disturbance in a Great Lakes forest. *Ecological Applications*, *23*(5), 1202–1215. https://doi.org/10.1890/12-1554.1

Guenther, A. B., Jiang, X., Heald, C. L., Sakulyanontvittaya, T., Duhl, T., Emmons, L. K., & Wang, X. (2012). The model of emissions of gases and aerosols from nature version 2.1 (MEGAN2.1): An extended and updated framework for modeling biogenic emissions. *Geoscientific Model Development*, *5*(6), 1471–1492. https://doi.org/10.5194/gmd-5-1471-2012

Hallquist, M., Wenger, J. C., Baltensperger, U., Rudich, Y., Simpson, D., Claeys, M., et al. (2009). The formation, properties and impact of secondary organic aerosol: Current and emerging issues. *Atmospheric Chemistry and Physics*, *9*(14), 5155–5236. https://doi.org/10.5194/acp-9-5155-2009

Hardacre, C., Wild, O., & Emberson, L. (2015). An evaluation of ozone dry deposition in global scale chemistry climate models. *Atmospheric Chemistry and Physics*, *15*(11), 6419–6436. https://doi.org/10.5194/acp-15-6419-2015

Harman, I. N., & Finnigan, J. J. (2007). A simple unified theory for flow in the canopy and roughness sublayer. *Boundary-Layer Meteorology*, *123*(2), 339–363. https://doi.org/10.1007/s10546-006-9145-6

Hoesly, R. M., Smith, S. J., Feng, L., Klimont, Z., Janssens-Maenhout, G., Pitkanen, T., et al. (2018). Historical (1750-2014) anthropogenic emissions of reactive gases and aerosols from the Community Emissions Data System (CEDS). *Geoscientific Model Development*, *11*(1), 369–408. https://doi.org/10.5194/GMD-11-369-2018

Holmes, C. D., Prather, M. J., & Vinken, G. C. M. (2014). The climate impact of ship NO_x emissions: An improved estimate accounting for plume chemistry. *Atmospheric Chemistry and Physics*, *14*(13), 6801–6812. https://doi.org/10.5194/acp-14-6801-2014

Horst, T. W. (1997). A simple formula for attenuation of eddy fluxes. *Boundary-Layer Meteorology*, *82*(2), 219–233. https://doi.org/10.1023/a:1000229130034

Hu, L., Millet, D. B., Baasandorj, M., Griffis, T. J., Turner, P., Helmig, D., et al. (2015). Isoprene emissions and impacts over an ecological transition region in the U.S. Upper Midwest inferred from tall tower measurements. *Journal of Geophysical Research: Atmospheres*, *120*(8), 3553–3571. https://doi.org/10.1002/2014JD022732

Hudman, R. C., Moore, N. E., Mebust, A. K., Martin, R. V., Russell, A. R., Valin, L. C., & Cohen, R. C. (2012). Steps towards a mechanistic model of global soil nitric oxide emissions: Implementation and space based-constraints. *Atmospheric Chemistry and Physics*, *12*(16), 7779–7795. https://doi.org/10.5194/acp-12-7779-2012

Jimenez, J. L., Canagaratna, M. R., Donahue, N. M., Prevot, A. S. H., Zhang, Q., Kroll, J. H., et al. (2009). Evolution of organic aerosols in the atmosphere. *Science (80-)*, *326*(5959), 1525–1529. https://doi.org/10.1126/science.1180353

Karl, M., Brauers, T., Dorn, H. P., Holland, F., Komenda, M., Poppe, D., et al. (2004). Kinetic study of the OH-isoprene and O_3-isoprene reaction in the atmosphere simulation chamber, SAPHIR. *Geophysical Research Letters*, *31*(5), 4–7. https://doi.org/10.1029/2003gl019189

Karlsson, P. E., Uddling, J., Braun, S., Broadmeadow, M., Elvira, S., Gimeno, B. S., et al. (2004). New critical levels for ozone effects on young trees based on AOT40 and simulated cumulative leaf uptake of ozone, Atmos. *The Environment Times*, *38*(15), 2283–2294. https://doi.org/10.1016/j.atmosenv.2004.01.027

Kavassalis, S. C., & Murphy, J. G. (2017). Understanding ozone-meteorology correlations: A role for dry deposition. *Geophysical Research Letters*, *44*(6), 2922–2931. https://doi.org/10.1002/2016GL071791

Kurpius, M. R., & Goldstein, A. H. (2003). Gas-phase chemistry dominates O_3 loss to a forest, implying a source of aerosols and hydroxyl radicals to the atmosphere. *Geophysical Research Letters*, *30*(7), 2–5. https://doi.org/10.1029/2002GL016785

Lammel, G. (1999). *Formation of nitrous acid: Parameterisation and comparison with observations* (Tech. Rep. 286). Max-Planck-Institut für Meteorologie. Retrieved from https://pure.mpg.de/pubman/faces/ViewItemOverviewPage.jsp?itemId=item_3187907

Langford, B., Acton, W., Ammann, C., Valach, A., & Nemitz, E. (2015). Eddy-covariance data with low signal-to-noise ratio: Time-lag determination, uncertainties and limit of detection. *Atmospheric Measurement Techniques*, *8*(10), 4197–4213. https://doi.org/10.5194/amt-8-4197-2015

Lee, X., Massman, W. J., & Law, B. (2005). Handbook of micrometeorology. *Handb. Micrometeorology*, *29*, 250.

Lei, Y., Yue, X., Liao, H., Gong, C., & Zhang, L. (2020). Implementation of yale interactive terrestrial biosphere model v1.0 into GEOS-Chem v12.0.0: A tool for biosphere-chemistry interactions. *Geoscientific Model Development*, *13*(3), 1137–1153. https://doi.org/10.5194/gmd-13-1137-2020

Lin, H., Jacob, D. J., Lundgren, E. W., Sulprizio, M. P., Keller, C. A., Fritz, T. M., et al. (2021). Harmonized Emissions Component (HEMCO) 3.0 as a versatile emissions component for atmospheric models: Application in the GEOS-Chem, NASA GEOS, WRF-GC, CESM2, NOAA GEFS-Aerosol, and NOAA UFS models. *Geoscientific Model Development*, *14*(9), 5487–5506. https://doi.org/10.5194/GMD-14-5487-2021

Lin, M., Malyshev, S., Shevliakova, E., Paulot, F., Horowitz, L. W., Fares, S., et al. (2019). Sensitivity of ozone dry deposition to ecosystem-atmosphere interactions: A critical appraisal of observations and simulations. *Global Biogeochemical Cycles*, *33*(10), 1264–1288. https://doi.org/10.1029/2018GB006157

Link, M. F., Pothier, M. A., Vermeuel, M. P., Riches, M., Millet, D. B., & Farmer, D. K. (2024). In-canopy chemistry, emissions, deposition, and surface reactivity compete to drive Bi-directional forest-atmosphere exchange of VOC oxidation products. *Environmental Science & Technology*, *1*(4), 305–315. https://doi.org/10.1021/acsestair.3c00074

Lombardozzi, D., Levis, S., Bonan, G., Hess, P. G., & Sparks, J. P. (2015). The influence of chronic ozone exposure on global carbon and water cycles. *Journal of Climate*, *28*(1), 292–305. https://doi.org/10.1175/JCLI-D-14-00223.1

Lombardozzi, D., Sparks, J. P., Bonan, G., & Levis, S. (2012). Ozone exposure causes a decoupling of conductance and photosynthesis: Implications for the Ball-Berry stomatal conductance model. *Oecologia*, *169*(3), 651–659. https://doi.org/10.1007/s00442-011-2242-3

Luhar, A. K., Woodhouse, M. T., & Galbally, I. E. (2018). A revised global ozone dry deposition estimate based on a new two-layer parameterisation for air-sea exchange and the multi-year MACC composition reanalysis. *Atmospheric Chemistry and Physics*, *18*(6), 4329–4348. https://doi.org/10.5194/acp-18-4329-2018

Makar, P. A., Staebler, R. M., Akingunola, A., Zhang, J., McLinden, C., Kharol, S. K., et al. (2017). The effects of forest canopy shading and turbulence on boundary layer ozone. *Nature Communications*, *8*, 1–14. https://doi.org/10.1038/ncomms15243

Marzuoli, R., Bussotti, F., Calatayud, V., Calvo, E., Alonso, R., Bermejo, V., et al. (2018). Dose-response relationships for ozone effect on the growth of deciduous broadleaf oaks in Mediterranean environment, Atmos. *The Environment Times*, *190*, 331–341. https://doi.org/10.1016/j.atmosenv.2018.07.053

Mauder, M., Cuntz, M., Drüe, C., Graf, A., Rebmann, C., Schmid, H. P., et al. (2013). A strategy for quality and uncertainty assessment of long-term eddy-covariance measurements. *Agricultural and Forest Meteorology*, *169*, 122–135. https://doi.org/10.1016/J.AGRFORMET.2012.09.006

Millet, D. B., Alwe, H. D., Chen, X., Deventer, M. J., Griffis, T. J., Holzinger, R., et al. (2018). Bidirectional ecosystem-atmosphere fluxes of volatile organic compounds across the mass spectrum: How many matter? *ACS Earth and Space Chemistry*, *2*(8), 764–777. https://doi.org/10.1021/acsearthspacechem.8b00061

Mills, G., Pleijel, H., Braun, S., Büker, P., Bermejo, V., Calvo, E., et al. (2011). New stomatal flux-based critical levels for ozone effects on vegetation. *Atmospheric Environment*, *45*(28), 5064–5068. https://doi.org/10.1016/j.atmosenv.2011.06.009

Monteith, J. L. (1965). Evaporation and environment. *Symposia of the Society for Experimental Biology*, 205–234.

Murray, L. T., Jacob, D. J., Logan, J. A., Hudman, R. C., & Koshak, W. J. (2012). Optimized regional and interannual variability of lightning in a global chemical transport model constrained by LIS/OTD satellite data. *Journal of Geophysical Research*, *117*(D20). https://doi.org/10.1029/2012JD017934

Neirynck, J., Gielen, B., Janssens, I. A., & Ceulemans, R. (2012). Insights into ozone deposition patterns from decade-long ozone flux measurements over a mixed temperate forest. *Journal of Environmental Monitoring*, *14*(6), 1684–1695. https://doi.org/10.1039/c2em10937a

Novak, G. A., Vermeuel, M. P., & Bertram, T. H. (2020). Simultaneous detection of ozone and nitrogen dioxide by oxygen anion chemical ionization mass spectrometry: A fast-time-response sensor suitable for eddy covariance measurements. *Atmospheric Measurement Techniques*, *1*(4), 1887–1907. https://doi.org/10.5194/amt-13-1887-2020

Ossola, R., & Farmer, D. (2024). The chemical landscape of leaf surfaces and its interaction with the atmosphere. *Chemical Reviews*, *124*(9), 1–96. https://doi.org/10.1021/acs.chemrev.3c00763

Philip, S., Martin, R. V., & Keller, C. A. (2016). Sensitivity of chemistry-transport model simulations to the duration of chemical and transport operators: A case study with GEOS-Chem v10-01. *Geoscientific Model Development*, *9*(5), 1683–1695. https://doi.org/10.5194/GMD-9-1683-2016

Rannik, Ü., Altimir, N., Mammarella, I., Bäck, J., Rinne, J., Ruuskanen, T. M., et al. (2012). Ozone deposition into a boreal forest over a decade of observations: Evaluating deposition partitioning and driving variables. *Atmospheric Chemistry and Physics*, *12*(24), 12165–12182. https://doi.org/10.5194/acp-12-12165-2012

Riches, M., Berg, T. C., Vermeuel, M. P., Millet, D. B., & Farmer, D. K. (2024). Wildfire smoke directly changes biogenic volatile organic emissions and photosynthesis of ponderosa pines. *Geophysical Research Letters*, *51*(6). https://doi.org/10.1029/2023GL106667

Ronda, R. J., De Bruin, H. A. R., & Holtslag, A. A. M. (2001). Representation of the canopy conductance in modeling the surface energy budget for low vegetation. *Journal of Applied Meteorology*, *40*(8), 1431–1444. https://doi.org/10.1175/1520-0450(2001)040<1431:ROTCCI>2.0.CO;2

Rummel, U., Ammann, C., Kirkman, G. A., Moura, M. A. L., Foken, T., Andreae, M. O., & Meixner, F. X. (2007). Seasonal variation of ozone deposition to a tropical rain forest in southwest Amazonia. *Atmospheric Chemistry and Physics*, *7*(20), 5415–5435. https://doi.org/10.5194/acp-7-5415-2007

Safieddine, S. A., Heald, C. L., & Henderson, B. H. (2017). The global nonmethane reactive organic carbon budget: A modeling perspective. *Geophysical Research Letters*, *44*(8), 3897–3906. https://doi.org/10.1002/2017GL072602

Seok, B., Helmig, D., Ganzeveld, L., Williams, M. W., & Vogel, C. S. (2013). Dynamics of nitrogen oxides and ozone above and within a mixed hardwood forest in northern Michigan. *Atmospheric Chemistry and Physics*, *13*(15), 7301–7320. https://doi.org/10.5194/acp-13-7301-2013

Shuttleworth, W. J., Gash, J. H. C., Lloyd, C. R., Moore, C. J., Roberts, J., Filho, A. D. O. M., et al. (1984). Eddy correlation measurements of energy partition for Amazonian forest. *Quarterly Journal of the Royal Meteorological Society*, *110*(466), 1143–1162. https://doi.org/10.1002/qj.49711046622

Silva, S. J., & Heald, C. L. (2018). Investigating dry deposition of ozone to vegetation. *Journal of Geophysical Research: Atmospheres*, *123*(1), 559–573. https://doi.org/10.1002/2017JD027278

Sitch, S., Cox, P. M., Collins, W. J., & Huntingford, C. (2007). Indirect radiative forcing of climate change through ozone effects on the land-carbon sink. *Nature*, *448*(7155), 791–794. https://doi.org/10.1038/nature06059

Stettler, M. E. J., Eastham, S., & Barrett, S. R. H. (2011). Air quality and public health impacts of UK airports. Part I: Emissions. *Atmospheric Environment*, *45*(31), 5415–5424. https://doi.org/10.1016/j.atmosenv.2011.07.012

Stevenson, D. S., Dentener, F. J., Schultz, M. G., Ellingsen, K., van Noije, T. P. C., Wild, O., et al. (2006). Multimodel ensemble simulations of present-day and near-future tropospheric ozone. *Journal of Geophysical Research*, *111*(D8). https://doi.org/10.1029/2005JD006338

Stevenson, D. S., Johnson, C. E., Collins, W. J., Derwent, R. G., Shine, K. P., & Edwards, J. M. (1998). Evolution of tropospheric ozone radiative forcing. *Geophysical Research Letters*, *25*(20), 3819–3822. https://doi.org/10.1029/1998GL900037

Stull, R. B. (1988). *An introduction to boundary layer meteorology* (pp. 427–428). Springer Science and Business Media.

Sun, S., Moravek, A., Trebs, I., Kesselmeier, J., & Sörgel, M. (2016). Investigation of the influence of liquid surface films on O_3 and PAN deposition to plant leaves coated with organic/inorganic solution. *Journal of Geophysical Research*, *121*(23), 1439–14256. https://doi.org/10.1002/2016JD025519

Sun, S., Tai, A. P. K., Yung, D. H. Y., Wong, A. Y. H., Ducker, J. A., & Holmes, C. D. (2022). Influence of plant ecophysiology on ozone dry deposition: Comparing between multiplicative and photosynthesis-based dry deposition schemes and their responses to rising CO_2 level. *Biogeosciences*, *19*(6), 1753–1776. https://doi.org/10.5194/bg-19-1753-2022

Tai, A. P. K., Martin, M. V., & Heald, C. L. (2014). Threat to future global food security from climate change and ozone air pollution. *Nature Climate Change*, *4*(9), 817–821. https://doi.org/10.1038/nclimate2317

Teiwes, R., Elm, J., Bilde, M., & Pedersen, H. B. (2019). The reaction of hydrated iodide I(H2O)- with ozone: A new route to IO2- products. *Physical Chemistry Chemical Physics*, *21*(32), 17546–17554. https://doi.org/10.1039/c9cp01734h

The International GEOS-Chem User Community. (2021). geoschem/GCClassic: GEOS-Chem 13.3.0. https://doi.org/10.5281/ZENODO.5703095

Travis, K. R., Jacob, D. J., Fisher, J. A., Kim, P. S., Marais, E. A., Zhu, L., et al. (2016). Why do models overestimate surface ozone in the southeastern United States? *Atmospheric Chemistry and Physics*, *16*, 2249–2262. https://doi.org/10.5194/acp-16-13561-2016

Univeristy of Michigan. (2023). Prophet AMOS 2016. Retrieved from https://www.dropbox.com/scl/fo/uks3rjb3e82w758sne4zb/h?dl=0

Vermeuel, M. P., Cleary, P. A., Desai, A. R., & Bertram, T. H. (2021). Simultaneous measurements of O_3 and HCOOH vertical fluxes indicate rapid in-canopy terpene chemistry enhances O_3 removal over mixed temperate forests. *Geophysical Research Letters*, *48*(3), e2020GL090996. https://doi.org/10.1029/2020GL090996

Vermeuel, M. P., Millet, D. B., Farmer, D. K., Ganzeveld, L. N., Visser, A. J., Alwe, H. D., et al. (2024). MLC-CHEM code and data for A vertically-resolved canopy improves chemical transport model predictions of ozone deposition to north temperate forests [Dataset]. *Data Repository for the University of Minnesota*. https://doi.org/10.13020/h966-ms14

Vermeuel, M. P., Millet, D. B., Farmer, D. K., Pothier, M. A., Link, M. F., Riches, M., et al. (2023). Closing the reactive carbon flux budget: Observations from dual mass spectrometers over a coniferous forest. *Journal of Geophysical Research: Atmospheres*, *128*(14), 1–20. https://doi.org/10.1029/2023JD038753

Vermeuel, M. P., Novak, G. A., Kilgour, D. B., Claflin, M. S., Lerner, B. M., Trowbridge, A. M., et al. (2023). Observations of biogenic volatile organic compounds over a mixed temperate forest during the summer to autumn transition. *Atmospheric Chemistry and Physics*, *23*(7), 4123–4148. https://doi.org/10.5194/acp-23-4123-2023

Visser, A. J., Ganzeveld, L. N., Finco, A., Krol, M. C., Marzuoli, R., & Boersma, K. F. (2022). The combined impact of canopy stability and soil NO_x exchange on ozone removal in a temperate deciduous forest. *Journal of Geophysical Research: Biogeosciences*, *127*(10), 1–16. https://doi.org/10.1029/2022JG006997

Visser, A. J., Ganzeveld, L. N., Goded, I., Krol, M. C., Mammarella, I., Manca, G., & Boersma, K. F. (2021). Ozone deposition impact assessments for forest canopies require accurate ozone flux partitioning on diurnal timescales. *Atmospheric Chemistry and Physics*, *21*(24), 18393–18411. https://doi.org/10.5194/acp-21-18393-2021

Wang, W., Ganzeveld, L., Rossabi, S., Hueber, J., & Helmig, D. (2020). Measurement report: Leaf-scale gas exchange of atmospheric reactive trace species (NO_2, NO, O_3) at a northern hardwood forest in Michigan. *Atmospheric Chemistry and Physics*, *20*(19), 11287–11304. https://doi.org/10.5194/acp-20-11287-2020

Wang, X., Jacob, D. J., Eastham, S. D., Sulprizio, M. P., Zhu, L., Chen, Q., et al. (2019). The role of chlorine in global tropospheric chemistry. *Atmospheric Chemistry and Physics*, *19*(6), 3981–4003. https://doi.org/10.5194/ACP-19-3981-2019

Wang, Y., Jacob, D. J., & Logan, J. A. (1998). Global simulation of tropospheric O_3-NO_x-hydrocarbon chemistry - 1. Model formulation. *Journal of Geophysical Research*, *103*(D9), 10713–10725. https://doi.org/10.1029/98jd00158

Wei, D., Alwe, H. D., Millet, D. B., Kavassalis, S. C., Lew, M., Bottorff, B., et al. (2020). Investigation of isoprene dynamics during the day-to-night transition period. *Journal of Geophysical Research: Atmospheres*, *125*(20), 1–15. https://doi.org/10.1029/2020JD032784

Wesely, M. L. (1989). Parameterization of surface resistances to gaseous dry deposition in regional scale numerical models. *Atmospheric Environment*, *7*(6), 961-1293–1304. https://doi.org/10.1016/S0950-351X(05)80241-1

Wild, O. (2007). Modelling the global tropospheric ozone budget: Exploring the variability in current models. *Atmospheric Chemistry and Physics*, *7*(10), 2643–2660. https://doi.org/10.5194/acp-7-2643-2007

Wolfe, G. M., & Thornton, J. A. (2011). The chemistry of atmosphere-forest exchange (CAFE) model - Part 1: Model description and characterization. *Atmospheric Chemistry and Physics*, *11*(1), 77–101. https://doi.org/10.5194/acp-11-77-2011

Wolfe, G. M., Thornton, J. A., McKay, M., & Goldstein, A. H. (2011). Forest-atmosphere exchange of ozone: Sensitivity to very reactive biogenic VOC emissions and implications for in-canopy photochemistry. *Atmospheric Chemistry and Physics*, *11*(15), 7875–7891. https://doi.org/10.5194/acp-11-7875-2011

Wong, A. Y. H., Geddes, J. A., Ducker, J. A., Holmes, C. D., Fares, S., Goldstein, A. H., et al. (2022). New evidence for the importance of non-stomatal pathways in ozone deposition during extreme heat and dry anomalies. *Geophysical Research Letters*, *49*(8), 1–12. https://doi.org/10.1029/2021GL095717

Wong, A. Y. H., Geddes, J. A., Tai, A. P. K., & Silva, S. J. (2019). Importance of dry deposition parameterization choice in global simulations of surface ozone. *Atmospheric Chemistry and Physics Discussions*, 1–41. https://doi.org/10.5194/acp-2019-429

Wu, Z., Schwede, D. B., Vet, R., Walker, J. T., Shaw, M., Staebler, R., & Zhang, L. (2018). Evaluation and intercomparison of five north American dry deposition algorithms at a mixed forest site. *Journal of Advances in Modeling Earth Systems*, *10*(7), 1571–1586. https://doi.org/10.1029/2017MS001231

Yanez-Serrano, A. M., Nölscher, A. C., Bourtsoukidis, E., Alves, E. G., Ganzeveld, L., Bonn, B., et al. (2018). Monoterpene chemical speciation in a tropical rainforest:variation with season, height, and time of dayat the Amazon Tall Tower Observatory (ATTO). *Atmospheric Chemistry and Physics*, *18*(5), 3403–3418. https://doi.org/10.5194/acp-18-3403-2018

Yienger, J. J., & Levy, H. (1995). Empirical model of global soil-biogenic NO_x emissions. *Journal of Geophysical Research*, *100*(D6), 11447–11464. https://doi.org/10.1029/95jd00370

Young, P. J., Naik, V., Fiore, A. M., Gaudel, A., Guo, J., Lin, M. Y., et al. (2018). Tropospheric ozone assessment report: Assessment of global-scale model performance for global and regional ozone distributions, variability, and trends. *Elementa*, *6*. https://doi.org/10.1525/elementa.265

Zhang, L., Brook, J. R., & Vet, R. (2003). A revised parameterization for gaseous dry deposition in air-quality models. *Atmospheric Chemistry and Physics*, *3*(6), 2067–2082. https://doi.org/10.5194/acp-3-2067-2003

Zhang, W., & Zhang, H. (2021). Secondary ion chemistry mediated by ozone and acidic organic molecules in iodide-adduct chemical ionization mass spectrometry. *Analytical Chemistry*, *93*(24), 8595–8602. https://doi.org/10.1021/acs.analchem.1c01486

Zhou, P., Ganzeveld, L., Taipale, D., Rannik, Ü., Rantala, P., Petteri Rissanen, M., et al. (2017). Boreal forest BVOC exchange: Emissions versus in-canopy sinks. *Atmospheric Chemistry and Physics*, *17*(23), 14309–14332. https://doi.org/10.5194/acp-17-14309-2017